INSILI 1 (2025) 100142

Contents lists available at ScienceDirect

In Silico Research in Biomedicine

journal homepage: www.sciencedirect.com/journal/in-silico-research-in-biomedicine

In-silico screening and molecular dynamics simulation of purpuride from *Talaromyces marneffei* strain SA2a: A potential inhibitor of *Burkholderia* virulence and drug resistance proteins

Alabi Peter Dare [a,b], Abideen Akinkunmi Wahab [a,b,*], Rahul Kumar Singh [c], Gbolahan Oladipupo Oduselu [d], Favour Emmanuel Adeloye [e], Deborah Temitope Olalekan [f], Folasade Muibat Adeyemi [a], Nana Aishat Yusuf-Omoloye [a], Rukayya Bushola Shittu [a]

[a] *Department of Microbiology, Osun State University, Osogbo, Nigeria*
[b] *African Centre of Excellence for Microbial Secondary Metabolites, Osun State University, Osogbo, Nigeria*
[c] *Department of Chemistry, University of North Bengal, District-Darjeeling, West Bengal, India*
[d] *West African Centre for Cell Biology of Infectious Pathogens (WACCBIP), University of Ghana, Accra, Ghana*
[e] *Department of Bioscience and Biotechnology, University of Medical Science, Ondo State, Nigeria*
[f] *Department of Biochemistry, Redeemer's University, Ede, Osun State, Nigeria*

ARTICLE INFO

Keywords:
ADMET properties
Burkholderia spp.
Drug resistance proteins
In-silico docking
MD Simulation
Purpuride

ABSTRACT

Burkholderia are Gram-negative bacteria that belong to two complexes, the *Burkholderia pseudomallei* complex and *Burkholderia cepacia* complex. These bacteria possess virulence and multidrug resistance properties that can prolong melioidosis and necrotizing pneumonia in infected patients. This study aims to investigate the activities of Purpuride on *Burkholderia* virulence and multidrug resistance proteins (BVDRP) using *in silico* molecular docking. Ligand and protein structures were obtained from PubChem and Research Collaboratory for Structural Bioinformatics database. Toxicity and pharmacokinetic properties of Purpuride and reference ligand 1-(1-naphthylmethyl)piperazine and Luteolin were predicted with ADMETlab and admetSAR online tools. Molecular docking was performed using CB-Dock2 online server, and interaction between the ligands and BVDRP was visualized with BIOVIA Discovery Studio Visualizer. Structural stability and interaction dynamics of the protein–ligand complexes were performed using GROMACS 2023.4 with the CHARMM36-jul2021 force field. Purpuride showed low toxicity and favourable pharmacokinetic properties. Purpuride demonstrated a good binding affinity -8.5 kcal·mol^{-1} with multidrug efflux transporter BpeB protein (7WLS), -7.5 kcal·mol^{-1} with BceF Tyrosine Kinase Domain protein (6Z0P), and formed strong interactions with amino acid residues compared to reference inhibitors. Structural stability analyses, including RMSD, RMSF, H-bond, and radius of gyration, indicated that Purpuride is stable with 7WLS, while Luteolin is the stable reference for 6Z0P, exhibiting minimal fluctuations and a compact conformation. The *in-silico* and MD simulations study suggests that Purpuride is a better inhibitor of 7WLS but a weak target for 6Z0P. Purpuride could serve as an alternative agent against drug resistance in *Burkholderia pseudomallei* infection.

1. Introduction

Burkholderia are Gram-negative bacteria belonging to two complexes, the *Burkholderia pseudomallei* complex (Bpc) and *Burkholderia cepacia* complex (Bcc) [1–4]. They consist of pathogenic and nonpathogenic groups of bacteria. *Burkholderia pseudomallei* has been reported as the cause of melioidosis in tropical and subtropical regions, characterized by high case fatality rates [3]. *Burkholderia cenocepacia* is an opportunistic pathogen, a member of the Bcc that affects individuals with compromised immune systems, especially those suffering from cystic fibrosis. The resistance of these pathogens to multiple antibiotics commonly used for *Burkholderia* infections makes treatment difficult [1, 3]. One of the significant factors contributing to multidrug resistance in *Burkholderia* spp. and other Gram-negative bacteria is the multidrug efflux mediated by the Resistance-Nodulation-Division (RND) superfamily tripartite transporter complex [3,5].

* Corresponding author at: Department of Microbiology, Osun State University, Osogbo, Nigeria.
E-mail address: abideen.wahab@uniosun.edu.ng (A.A. Wahab).

https://doi.org/10.1016/j.insi.2025.100142
Received 29 September 2025; Received in revised form 12 November 2025; Accepted 25 November 2025
Available online 26 November 2025

BpeF and BpeB form BpeEF-OprC and BpeAB-OprB tripartite complexes, which contribute to multidrug resistance in *B. pseudomallei*. The BpeB is homologous to AcrB (65 % identity and 88 % similarity) in *Escherichia coli* and MexB (62 % identity and 87 % similarity) in *Pseudomonas aeruginosa* [3,6–8]. BpeB is reported to export tetracyclines, fluoroquinolones, and macrolides as substrates. BpeF shows higher amino acid sequence homology (60 % identity and 85 % similarity) to OqxB in *Klebsiella pneumoniae* than MexB and AcrB [3]. BpeF confers resistance to sulfamethoxazole, trimethoprim, chloramphenicol, tetracycline, and fluoroquinolones [1,3]. The efflux pumps BpeB and BpeF are not only conserved in *B. pseudomallei* complex species but also Bcc species [3,9].

Burkholderia invasion protein (BipD) is a dumbbell-shaped protein at the *Burkholderia* secretion apparatus (Bsa) needle tip. BipD serves as a platform for the assembly of the translocon pore with *Burkholderia* invasion protein B (BipB) (a major translocon protein) and *Burkholderia* invasion protein C (BipC) (a minor translocon protein). It enables the direct passage of effector proteins from the cytoplasm of *B. pseudomallei* into the target host cell. The effector proteins suppress host cell processes to benefit the bacteria [10,11]. BipD plays a vital role in promoting the intracellular replication and survival of B. pseudomallei by enabling it to escape from phagosomes. BipD is a protein that can be categorized as a virulence factor due to its ability to enable the bacterium to invade non-phagocytic cells, escape from the phagosome, and induce intracellular replication. The bacterium also forms actin tails, causing cell-to-cell spread, thus allowing survival of extracellular environment and evade both host defenses and antibiotic treatment [10].

Bacterial tyrosine kinases (BY-kinases) are enzymes present in both Gram-negative and Gram-positive bacteria, controlling a broad spectrum of metabolic pathways and regulatory mechanisms, such as the metabolism of polysaccharides, DNA metabolism, stress response, and virulence [12–14]. BY-kinases serve as key regulators of biofilm formation and virulence [14,15]. The *bceF* gene in *B. cepacia* encodes for the protein tyrosine kinase BceF, which is required for the biosynthesis of the exopolysaccharide, as reduced biofilm formation was seen in *B. cepacia bceF* mutant strain [14,16].

β-lactamases are classified into four different classes based on structural similarities (A–D). Class A, C, and D enzymes contain an active-site serine, as the nucleophile, and class B β-lactamases are metalloenzymes using one or two Zn^{2+} ions for catalysis. PenA and PenI are class A β-lactamases which mediate resistance to β-lactams in *Burkholderia*. Bcc and Bpc bacteria contain chromosomally encoded representatives of class A, C, and D β-lactamases. Bcc bacteria encode two annotated class A β-lactamases, PenA and PenB, as well as the class C enzyme AmpC [17,18].

The enzyme dihydropteroate synthase (DHPS) catalyses the reaction of 6-hydroxymethyl-7,8-dihydropterin-pyrophosphate with p-aminobenzoic acid (p-ABA) to yield 7,8-dihydropteroate and pyrophosphate. The enzyme facilitates the biosynthesis of folate, a crucial metabolite necessary for the synthesis of DNA and proteins. The folate pathway comprises of many enzymes in addition to DHPS, including 6-hydroxymethyl-7,8-dihydropterin pyrophosphokinase (HPPK), dihydrofolate synthetase (DHFS) and dihydrofolate reductase (DHFR) [19]. DHPS is a validated drug target for treating diseases caused by bacteria and protozoan parasites. Sulfonamides, in particular, are inhibitors of this enzyme and are used as antibiotics. However, increasing levels of resistance to sulfonamides have been observed, and new drug development is needed [19–21].

The peptidoglycan-associated lipoprotein (Pal) is an immunogenic protein that has been consistently identified in *B. multivorans* and *B. cenocepacia*. Pal from both species generated pronounced antibody responses in Bcc infected patients. Lipoproteins play roles in the pathogenesis of various bacterial species, as they are involved in signal transduction, conjugation, and nutrient uptake, and also contribute to antibiotic resistance, protein transport, and extracytoplasmic protein folding [22]. Lipoproteins also facilitate bacterial adhesion, invasion, colonization, immunomodulation and evasion of host defence. Pal is a component of the Tol-Pal system, which comprises the five core proteins TolQ, TolR, TolA, TolB, and Pal. The Tol-Pal proteins form a complex that spans the inner and outer membranes and is required for maintaining cell wall integrity, which can be exploited for the entry of macromolecules, such as bacteriocins and bacteriophages [22,23].

Bacterial porins have been classified into non-specific (general diffusion) and specific porins. Non-specific porins allow the passage of hydrophilic solutes and exhibit a linear relationship between the permeation rate and the solute concentration gradient [24,25]. On the other hand, specific porins exhibit Michaelis–Menten kinetics for the transport of specific solutes. Outer membrane porin in *Burkholderia pseudomallei* is a crucial component of the bacterial outer membrane, playing a key role in regulating membrane permeability and influencing the susceptibility of *B. pseudomallei* to various antimicrobial agents, particularly carbapenems and cephalosporins [25].

A thorough search of the literature revealed no known specific inhibitors of *Burkholderia* virulence and drug resistance proteins, as research is still ongoing to develop and establish specific, effective inhibitors for these proteins.

Red pigment of *Talaromyces* species has been reported to exhibit a wide range of biological activities, including antibacterial, anti-inflammatory, and antitumor properties [26]. We previously reported the anti-biofilm formation and inhibitory potential of Purpuride pigment from *Talaromyces marneffei* strain SA2a on multidrug-resistant *Burkholderia* spp [1]. As previously mentioned, *Burkholderia pseudomallei* is the causative agent of melioidosis in tropical and subtropical regions, characterized by high case fatality rates. Likewise, *Burkholderia cepacia* affects individuals with compromised immune systems, particularly those suffering from cystic fibrosis. Targeting virulence and drug resistance proteins will help to reduce drug resistance and virulence activities of these pathogens. To understand the mechanism of action of Purpuride, evaluating *in silico* molecular docking of Purpuride on *Burkholderia* virulence and multidrug resistance proteins will help predict the mechanisms of action of this pigment, which will aid in developing a potential specific inhibitor of *Burkholderia* virulence and drug resistance proteins that will help to overcome drug resistance in *Burkholderia* sp.

2. Materials and methods

2.1. In silico molecular docking of compounds

In silico molecular docking studies were performed to understand the interaction of Purpuride pigment from *Talaromyces marneffei* strain SA2a with virulence and multidrug resistance proteins in *Burkholderia* isolates, with modifications to the method described by [27–32].

2.1.1. Selection of compounds for in silico study

Purpuride compound used in this study was obtained from the report of [1], who identified red pigment of *Talaromyces marneffei* strain SA2a using UV-visible spectroscopy, Fourier Transform Infrared Spectroscopy (FTIR), Gas Chromatography-Mass Spectrometry (GC-MS) analysis as Purpuride pigment, and evaluated the pigment's inhibitory potential on Multidrug-resistant *Burkholderia* sp. A thorough review of the literature revealed no known specific inhibitors of *Burkholderia* virulence, and drug resistance proteins have been previously reported. However, based on previous reports [33–36], other known inhibitors of drug resistance proteins in Gram-negative bacteria, with a similar mechanism of action and inhibitory effects on *Burkholderia* virulence and drug resistance proteins, were selected for this study.

2.1.2. Protein preparation

Three-dimensional (3D) protein structures of *Burkholderia* virulence and multidrug resistance receptors Table 1 were obtained from the protein data bank of the RCSB (https://www.rcsb.org/) and Protein Data Bank Japan (https://pdbj.org/).

Table 1
List of Bcc and Bpc virulence and multidrug resistance proteins.

Burkholderia pseudomallei complex			*Burkholderia cepacia* complex		
Targets	PDB ID	Ref.	Targets	PDB ID	Ref.
BipD of B. *pseudomallei*	2IXR	[37]	Beta-lactamase	5HX9	[39]
Outer membrane porin (BpsOmp38)	8WV0	[38]	Peptidoglycan-associated lipoprotein	5LKW	[22]
Multidrug efflux transporter BpeB	7WLS	[3]	Dihydropteroate synthase (folP)	2Y5J	[19]
Multidrug efflux transporter BpeF	7WLV	[3]	BceF Tyrosine Kinase Domain	6Z0P	[14]

Key PDB ID -Protein Data Bank Identity, Bpc -*Burkholderia pseudomallei* complex, Bcc- *Burkholderia capacia* complex.

2.1.3. Homology modelling of protein targets

The crystal structures of some of the selected protein targets exhibited incomplete regions within the polypeptide chains, necessitating homology modeling to reconstruct missing residues prior to molecular docking and molecular dynamics simulations. Homology models were generated using the SWISS-MODEL server (https://swissmodel.expasy.org/) [40], which employs a fully automated template-based modelling approach. Proteins were prepared using Discovery Studio v21.1.0.20298 by removing crystallographic water molecules and heteroatoms, correcting missing residues, and assigning protonation states appropriate for pH 7.4.

2.1.3.1. Homology model validation. After homology modeling and energy minimization, the predicted structures of proteins were validated using the SAVES v6.1 server (https://saves.mbi.ucla.edu/). Each model was uploaded to the platform, which integrates several independent quality assessment tools, including PROCHECK, ERRAT, and VERIFY3D, to evaluate overall structural integrity. PROCHECK assessed stereochemical geometry by analyzing φ (phi) and ψ (psi) torsion angles and generating Ramachandran plots, along with G-factors, to verify backbone conformational quality. ERRAT examined non-bonded atomic interactions between C, N, and O atoms, providing an overall quality factor, where scores above 80 % indicate reliable models [41]. VERIFY3D evaluated 3D–1D sequence compatibility by analyzing residue environments (secondary structure, polarity, and solvent accessibility) using a 21-residue sliding window [42]. Models with >80 % of residues scoring ≥0.2 were considered structurally valid and suitable for downstream computational analyses.

2.1.4. Ligand preparation

Three-dimensional (3D) conformation Ligand structure of Purpuride from *Talaromyces marneffei* strain SA2a, previously reported by [1] with slight modification, was prepared and geometry-optimized using the MMFF94 force field [43], after being obtained from the PubChem database (https://pubchem.ncbi.nlm.nih.gov/), Table 2.

2.1.5. Molecular docking and visualization of interactions

Molecular docking was performed to predict binding affinity and pose using CB-Dock2 online server (https://cadd.labshare.cn/cb-dock2/index.php) [44], which integrates a cavity-detection algorithm with AutoDock Vina. For each ligand–protein pair, CB-Dock2 automatically identified potential binding cavities and generated grid boxes around the highest-volume cavities. Docking was carried out with default parameters, and binding scores were reported without a reference ligand in kcal·mol^{-1}. The top-ranked docked poses were analyzed in BIOVIA Discovery Studio Visualizer to identify the interactions that occur during binding between Purpuride and the proteins.

Table 2
Identity of purpuride pigment from *Talaromyces marneffei* strain SA2a [1].

S/N	PubChem CID	Area (%)	Library/ID	Molecular Formula	M/Z
1	101316833	3.70	Purpuride	$C_{22}H_{33}NO_5$	391.5

2.2. ADMET properties of Purpuride and reference ligands

According to the method described by [45], with slight modifications, ADMETlab 3.0 (https://admetlab3.scbdd.com/server/evaluation) was used to predict the absorption, distribution, metabolism, excretion, and toxicity (ADMET) of the compounds. The pharmacokinetic properties and the toxicity of the compound were predicted.

2.3. Comparison of molecular docking of Purpuride with reference inhibitors

The *Burkholderia pseudomallei* and *Burkholderia cepacia* virulence and drug resistance proteins that showed the highest binding affinity and top-scoring pose with Purpuride were further selected for molecular docking and molecular dynamics simulation studies with a reference ligand for comparison and validation of their stability as potential inhibitors. Crystal structures of the protein targets BceF Tyrosine Kinase Domain (6Z0P) in *Burkholderia cepacia* and Multidrug efflux transporter BpeB from *Burkholderia pseudomallei* (7WLS) were used for the comparison studies based on their binding affinity and interactions with Purpuride. Positive control ligands Luteolin (PubChem CID 5280445), a known inhibitor of tyrosine kinase activity, and 1-(1-Naphthylmethyl) piperazine (PubChem CID 701891), a known inhibitor of efflux pump and can reverse multidrug resistance in Gram-negative bacteria, were retrieved from PubChem and serve as reference ligands for the 6Z09 and 7WLS. Molecular docking was performed to predict the binding affinity using CB-Dock2 online server as described above [44]. The top-ranked docked poses were analyzed in BIOVIA Discovery Studio Visualizer to identify the interactions that occur during binding between Purpuride, reference ligands, and the proteins. The top-scoring pose was used for subsequent MD simulation analysis.

2.4. Molecular dynamic simulation over 100ns

Molecular dynamics (MD) simulations were performed using GROMACS 2023.4 with the CHARMM36-jul2021 force field [46,47] to investigate the structural stability and interaction dynamics of protein–ligand complexes. Each docked complex was solvated in a triclinic box using the TIP3P water model [48], and counterions were added to neutralize the system. Periodic boundary conditions were applied in all three spatial dimensions. Prior to equilibration, energy minimization was carried out using the steepest descent algorithm for a maximum of 50,000 steps, or until the maximum force reached 1000 kJ/mol/nm. Non-bonded interactions were treated with the Verlet cutoff scheme, where both electrostatics and van der Waals interactions were truncated at 1.2 nm. Long-range electrostatics were described using the Particle Mesh Ewald (PME) method with a grid spacing of 0.16 nm.

Following minimization, the systems were equilibrated in two stages, with positional restraints applied to the protein and ligand. First, NVT equilibration was conducted for 1 ns at 300 K using the V-rescale thermostat with a coupling constant of 0.1 ps to stabilize the system temperature. This was followed by NPT equilibration for 1 ns at 300 K and 1 bar. Pressure control was initially maintained using the Berendsen barostat and subsequently stabilized with the Parrinello–Rahman scheme, employing a coupling constant of 2.0 ps and a compressibility of 4.5×10^{-5} bar^{-1}.

After equilibration, a 100 ns production MD run was performed for each complex under NPT conditions [49]. Simulations were carried out for 50,000,000 steps with a 2 fs timestep, where bond constraints were applied using the LINCS algorithm to fix all bonds involving hydrogen atoms. Electrostatic interactions were calculated with the PME method,

and van der Waals interactions were smoothly switched off between 1.0 and 1.2 nm using a force-switch function. Coordinates, velocities, and energies were saved every 10 ps throughout the simulation.

Trajectory analyses were carried out using GROMACS utilities to evaluate the root-mean-square deviation (RMSD), root-mean-square fluctuation (RMSF), radius of gyration (Rg), solvent accessible surface area (SASA), and hydrogen bonding patterns, thereby allowing detailed assessment of the conformational stability of the proteins and persistence of the ligands within their binding pockets. The MD simulation parameters used for protein–ligand complexes are presented in **Table A.1**.

2.5. Density functional theory study

The quantum chemical calculations of all three ligands were performed using Gaussian 09 software package. The ground-state geometries of Luteolin, 1-(1-naphthylmethyl)piperazine, and Purpuride were optimized employing Density Functional Theory (DFT) with the Becke's three-parameter hybrid functional (B3LYP) [50] in combination with the 6–31 G basis set. Geometry optimization was carried out without imposing any symmetry constraints, and full structural relaxation was achieved until the root mean square (RMS) force convergence criteria were satisfied. The geom = connectivity keyword was applied to preserve molecular connectivity during optimization. The optimization step ensured that each ligand attained its most stable conformer at the given level of theory.

All computations were performed in the gas phase at 298 K. The optimized geometries were further used to derive frontier molecular orbital (FMO) distributions, including highest occupied molecular orbital (HOMO) and lowest unoccupied molecular orbital (LUMO) energies, which provided insights into the electronic properties and chemical reactivity of the ligands.

3. Results and discussion

3.1. Preparation of ligands and protein receptors

The structure of Purpuride and reference ligand 1-(1-Naphthylmethyl)piperazine and Luteolin obtained from PubChem database Fig. 1 and the 3D structure of the *Burkholderia* virulence and drug resistance proteins from RCSB and Protein Data Bank Japan are shown in Figs. 2a and 2b.

The resistance of *Burkholderia* spp. to multiple antibiotics commonly used for treating infections caused by *Burkholderia* makes the treatment

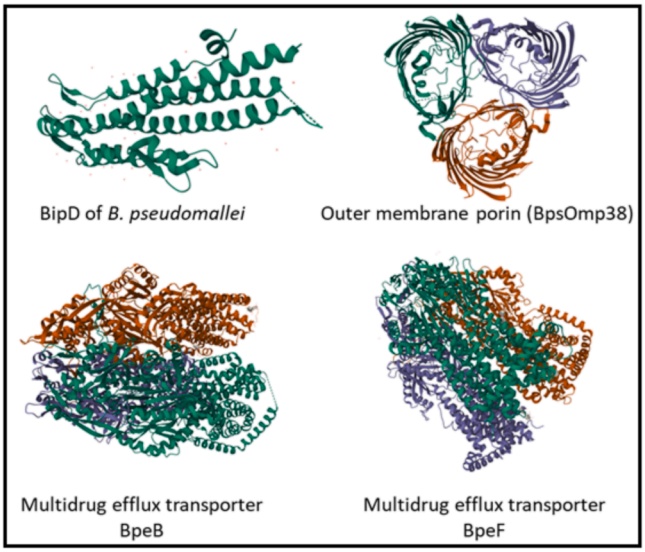

Fig. 2a. 3D crystal structure of *Burkholderia pseudomallei* virulence and drug resistance proteins.

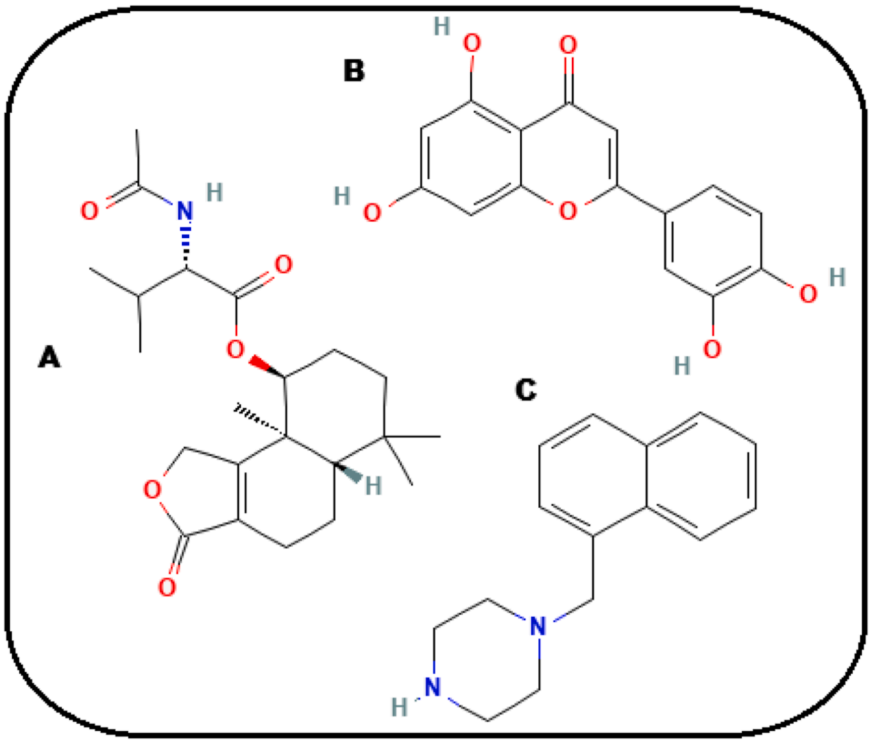

Fig. 1. 2D structure of (A) Purpuride (B) Luteolin (C) 1-(1-Naphthylmethyl)piperazine selected for *in silico* and molecular dynamics simulations with *Burkholderia* virulence and drug resistance proteins.

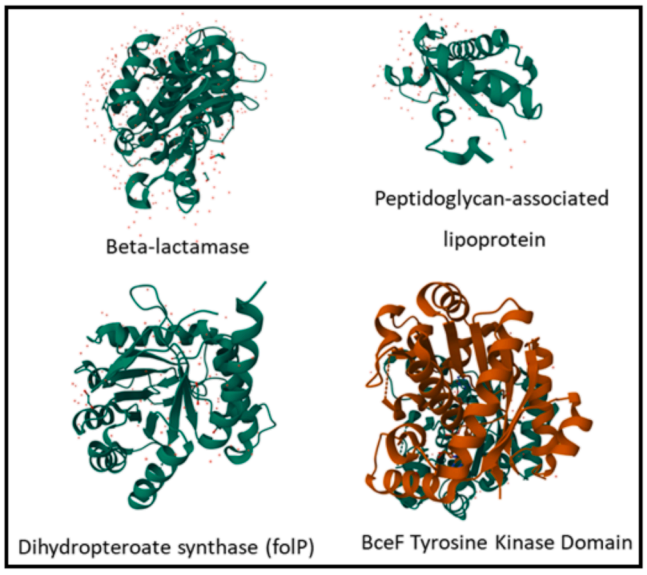

Fig. 2b. 3D crystal structure of *Burkholderia cepacia* virulence and drug resistance proteins.

of these infections difficult [1]. One of the significant factors contributing to multidrug resistance in *Burkholderia* spp. and other Gram-negative bacteria is the virulence properties and multidrug efflux by the Resistance-Nodulation-Division (RND) superfamily tripartite transporter complex [3,5].

3.2. Homology modeling results

To address missing residues in the crystal structures of the selected protein targets, which have incomplete regions within the polypeptide chains (6Z0P and 7WLS), homology modeling was performed using the SWISS-MODEL server. The resulting models were evaluated for stereochemical quality using MolProbity and QMEANDisCo scores, which provide quantitative benchmarks for structural accuracy and reliability. The refined 6Z0P homology model achieved a MolProbity score of 0.98, indicating a high-quality structural model comparable to those from high-resolution crystal structures. The clash score was exceptionally low (1.17), with only minor steric overlaps observed (notably involving residue A120 ARG with ADP). The Ramachandran analysis revealed that 97.14 % of residues fell within the favoured regions, with no outliers, indicating a well-refined backbone geometry. Only 0.73 % of side-chain rotamers were identified as outliers (A100 LEU, A78 LYS, A177 ARG), reflecting minimal side-chain strain. No Cβ deviations were detected, and only 4 out of 3859 bonds and 14 out of 5240 bond angles were flagged as outliers, mainly associated with flexible loop regions or ligand contacts. The QMEANDisCo global score was 0.92 ± 0.05, further confirming strong structural reliability. Subcomponents of QMEAN, including solvation (1.43) and torsion (1.64), reinforced the overall structural consistency.

The homology model for 7WLS also exhibited excellent quality, with a MolProbity score of 0.95 and a very low clash score (0.80), suggesting a stereochemically sound model. The Ramachandran plot showed 96.77 % of residues in favored regions, with a minimal 0.23 % of residues classified as outliers (including C504 HIS, A754 SER, and C632 ASP), reflecting strong overall backbone geometry. Rotamer outliers were limited to 0.83 %, involving a small set of side chains (e.g., C829 GLN, C692 ASP). Some deviations were observed in Cβ geometry (36 instances) and a moderate number of bad bonds (4/23938) and bad angles (138/32598), consistent with the complexity of this large membrane-associated protein. Three cis-prolines and one twisted non-proline bond were identified, which may represent biologically relevant local strain. The QMEANDisCo global score was 0.87 ± 0.05, slightly lower than 6Z0P but still within the acceptable range for reliable structural models. Subscores highlighted reasonable solvation (0.96) and torsion (−0.55) components, consistent with the expected conformational flexibility of this transporter protein shown in **Table A.2.**

3.2.1. Structural validation of the homology models

The stereochemical quality and structural reliability of the modeled proteins 6Z0P and 7WLS were evaluated using PROCHECK, ERRAT, and VERIFY3D via the SAVES v6.1 server (UCLA, USA) **Table A.3 & Supplementary Material 1**. These analyses confirmed that both models possess high structural accuracy, proper residue environments, and minimal errors, making them suitable for molecular docking and dynamics studies.

PROCHECK analysis revealed excellent stereochemical geometry, with 92.8 % (6Z0P) and 91.2 % (7WLS) of residues located in the most favoured regions of the Ramachandran plot, and no residues in disallowed regions. The G-factor values (−0.0 for 6Z0P and −0.1 for 7WLS) were within the acceptable range, confirming that the backbone dihedral angles and bond geometries closely resemble those of experimentally determined protein structures.

ERRAT evaluation yielded overall quality factors of 92.1 % (6Z0P) and 89.7 % (7WLS), both exceeding the 80 % benchmark indicative of high-quality models. These values suggest that the non-bonded atomic interactions in the predicted structures are consistent with those observed in experimentally solved proteins, with minor variations confined to flexible loop regions.

VERIFY3D further validated the models' reliability, with 91.4 % (6Z0P) and 90.6 % (7WLS) of residues scoring ≥0.2 in the 3D–1D compatibility analysis. This high percentage confirms that most residues occupy appropriate structural environments consistent with their physicochemical properties and sequence context.

3.3. ADMET properties of Purpuride and reference ligands

The ADMET properties of Purpuride and reference ligand 1-(1-Naphthylmethyl)piperazine and Luteolin were evaluated using ADMETlab and admetSAR analysis. The pharmacokinetics revealed that the compounds exhibited excellent human intestinal absorption. Meanwhile, Purpuride and Luteolin showed poor Caco-2 Permeability and Plasma protein binding activities. Additionally, Purpuride demonstrated poor properties as a P-glycoprotein inhibitor. Furthermore, Purpuride and the reference ligand 1-(1-Naphthylmethyl)piperazine showed poor half-life properties. The selected compounds did not inhibit CYP3A4, CYP2C9, or CYP2D6 enzymes. However, the compound Purpuride cannot cause Human Ether-a-go-go-Related Gene inhibition, and showed good properties for eye corrosion and eye irritation, drug-induced nephrotoxicity, drug-induced neurotoxicity, and AMES toxicity, unlike the reference ligands Table 3. Although some poor pharmacokinetic properties were observed in the selected compounds, the results of this study suggest that the compounds could be considered as promising agents for potential application in pharmaceutical industry. The result of this study is similar to the ADMET and pharmacokinetics properties of Uridine triphosphate (UTP) (CID 6133) reported by [29], who identified in his study that the UTP can be easily absorbed from the gastrointestinal tract by the cellular transport mechanism, not permeable to the blood-brain barrier (BBB) shield of the brain. Least synthetic accessibility. Similarly, triazolo [4, 3-b] pyridazin-3-yl-quinoline derivatives reported by [51] demonstrated good volume distribution (VDs) in the range of 0.04–20 L/kg, can permeate through the BBB, and did not inhibit cytochrome P450 enzymes (CYP1A2, CYP3A4, CYP2C19, CYP2D6, and CYP2C9).

Table 3
ADMET properties of Purpuride and reference ligands.

Properties (value/ probability)	Purpuride	1-(1-Naphthylmethyl) piperazine	Luteolin
Absorption			
Human intestinal absorption	(Ex) —	(Ex) —	(Ex) —
Caco-2 Permeability	(Poor) -5.346	(Ex) -4.909	(Poor) -5.192
P-glycoprotein inhibitor	(Poor) +++	(Ex) —	(Ex) —
P-glycoprotein substrate	(Ex) —	(Med) +	(Ex) –
F20 %	(Ex) –	(Ex) –	Poor) +++
F30 %	(Ex) –	(Ex) –	Poor) +++
F50 %	(Poor) +++	(Ex) –	Poor) +++
Distribution			
Plasma protein binding (%)	(Poor) 94.7 %	(Ex) 65.2 %	(Poor) 97.6 %
VDss	(Ex) 0.834	(Ex) 0.736	(Ex) 0.243
Blood Brain Barrier	(Ex) —	(Med) -	Ex) —
Fu	(Ex) 5.5 %	(Ex) 32.0 %	(Poor) 2.3 %
Metabolism			
CYP3A4 inhibitor	(Ex) —	(Ex) —	(Poor) +++
CYP3A4 substrate	(Ex) —	(Poor) +++	(Ex) —
CYP2C9 inhibitor	(Ex) —	(Ex) —	(Ex) —
CYP2C9 substrate	(Ex) —	(Ex) —	(Ex) –
CYP2D6 inhibitor	(Ex) —	(Poor) ++	(Med) +
CYP2D6 substrate	(Ex) —	(Ex) —	(Poor) +++
HLM Stability	(Med) +	(Poor) —	(Ex) ++
Excretion			
CLplasma	(Med) 5.315	(Med) 7.758	(Med) 8.482
T1/2	(Poor) 0.696	(Poor) 0.814	(Med) 1.373
Toxicity			
hERG Blockers	(Ex) 0.014	(Poor) 0.788	(Ex) 0.069
hERG Blockers (10um)	(Ex) 0.088	(Poor) 0.762	(Med) 0.61
AMES Toxicity	(Ex) 0.121	(Med) 0.574	(Med) 0.65
Eye Corrosion	(Ex) 0.002	(Poor) 0.939	(Med) 0.464
Eye Irritation	(Ex) 0.156	(Poor) 0.869	(Poor) 0.998
Drug-induced Nephrotoxicity	(Ex) 0.0367	(Poor) 0.906	(Ex) 0.01
Drug-induced Neurotoxicity	(Ex) 0.0213	(Poor) 0.979	(Ex) 0.012
Ototoxicity	(Med) 0.605	(Med) 0.373	(Ex) 0.153
Hematotoxicity	(Med) 0.484	(Med) 0.432	(Ex) 0.029
RPMI-8226 Immunitoxicity	(Ex) 0.098	(Ex) 0.045	(Ex) 0.025
A549 Cytotoxicity	(Ex) 0.151	(Ex) 0.13	(Med) 0.669
Hek293 Cytotoxicity	(Ex) 0.184	(Ex) 0.288	(Med) 0.694

Key: EX- Excellent, Med- Medium.

3.4. Molecular docking of Purpuride with Burkholderia virulence and drug resistance proteins

The molecular docking results showed the interaction of Purpuride with BipD of *B. pseudomallei*, Outer membrane porin (BpsOmp38), Multidrug efflux transporter BpeB, Multidrug efflux transporter BpeF VDRP in *Burkholderia pseudomallei,* as well as interaction with Beta-lactamase, Peptidoglycan-associated lipoprotein, Dihydropteroate synthase (folP), BceF Tyrosine Kinase Domain VDRP in *Burkholderia cepacia*. The results of this study are similar to the report of [29], who reported molecular docking of six compounds (CID: 25390206, 28359984, 284262, 284264, 6133, and 8900795) as potential inhibitors of Uridine monophosphate/Uridylate (UMP) kinase.

Similarly, [52] evaluated *in silico* molecular docking of newly synthesized compounds from the reaction of quinazolinone chalcones either with 2-amino aniline in acidic medium to give diazepines or with 2-aminophenol to offer oxazepane against the outer membrane protein A (OMPA), exo-1,3-beta-glucanase for their antimicrobial activity and antitumor signalling inhibition. In addition, [27] investigated *in silico* molecular docking of six (6) compounds (Patulin, Leucodelphinidin, Quercetin, Taxifolin Kaempferol, and Isofraxidin) derived from endophytic *Penicillium setosumon* on nine (9) antibacterial protein targets (DNA gyrase, β-ketoacyl ACP reductase (FabG), 3R-hydroxyacyl ACP dehydratase (FabZ), trans 2- enoyl ACP reductase (FabI), D-alanine: D-alanine ligase (Ddl), dihydropteroate synthase (DHPS), penicillin binding protein (PBP)and Elongation factor Tu (EF Tu) and 16S rRNA A site).

3.4.1. Interaction of Purpuride with Burkholderia pseudomallei virulence and drug resistance proteins

The molecular docking study revealed interactions of Purpuride with *Burkholderia pseudomallei* VDRP. On all the docked proteins, it was observed that Purpuride had binding affinity of −8.6 kcal·mol^{-1} with multidrug efflux transporter BpeF, −8.5 kcal·mol^{-1} with multidrug efflux transporter BpeB protein, −7.4 kcal·mol^{-1} outer membrane porin (BpsOmp38), and −6.1 kcal·mol^{-1} BipD of *B. pseudomallei,* respectively, Table 4a.

The interactions of Purpuride with these proteins indicated that conventional hydrogen bonds were formed with amino acids ARG619 and GLN292, and carbon hydrogen bonds with SER134, GLY618, and LYS814, and an unfavourable acceptor-acceptor bond was seen with GLN44 at the active site of the multidrug efflux transporter BpeB protein chain A. Purpuride also formed a conventional hydrogen bond with THR149 at the active site of BipD of *B. pseudomallei* chain A. In addition, Purpuride interacted with amino acid VAL402 and LEU996 with an alkyl bond and a conventional hydrogen bond with ARG1007 at the active site of the Multidrug efflux transporter BpeF chain B. Furthermore, Purpuride also interacted with ARG41 and 80 with a conventional hydrogen bond and an alkyl bond with PRO108 at the active site of Outer membrane porin (BpsOmp38) protein chain B. Fig. 3a. The coordinates of *Burkholderia pseudomallei* VDRP interactions with Purpuride are shown in **Table A.4a.**

In this study, Purpuride formed an alkyl, pi-alkyl, a pi-sigma, and a conventional hydrogen bond with amino acids at the active site of *Burkholderia pseudomallei* VDRP. The strong binding affinity of this Purpuride to *Burkholderia pseudomallei* VDRP may be due to the compound forming bonds that interact with the amino acids of the proteins, which may prevent amino acid expression, making it a promising inhibitor of *Burkholderia pseudomallei* VDRP. This is in line with the report of [29], who reported that UTP (CID 6133) had the highest docking score of −8.7 kcal/mole followed by 4-(2-Amino-4-(4--chlorophenyl)-7-oxo-5H-pyrrolo[3,4-d]pyrimidin-6(7H)-yl)butanoic acid (CID 284262) with −8.1 kcal·mol^{-1} on UMP kinase in *Burkholderia pseudomallei*. In a similar study, molecules leucodelphinidin and dihydroquercetin showed maximum affinity to (DNA gyrase, β-ketoacyl ACP reductase (FabG), 3R-hydroxyacyl ACP dehydratase (FabZ), trans 2-enoyl ACP reductase (FabI), D-alanine:D-alanine ligase (Ddl), dihydropteroate synthase (DHPS), penicillin binding protein (PBP), and 16S rRNA A site) except 1OB2 (elongation factor TU) [27].

Table 4a
Binding affinity of Purpuride with *Burkholderia pseudomallei* VDRP.

Burkholderia pseudomallei complex		
Ligand	Targets	Binding Affinity (kcal·mol^{-1})
Purpuride	BipD of B. *pseudomallei*	−6.1
	Outer membrane porin (BpsOmp38)	−7.4
	Multidrug efflux transporter BpeB	−8.5
	Multidrug efflux transporter BpeF	−8.6

Key: kcal·mol^{-1}- Kilocalorie per mole.

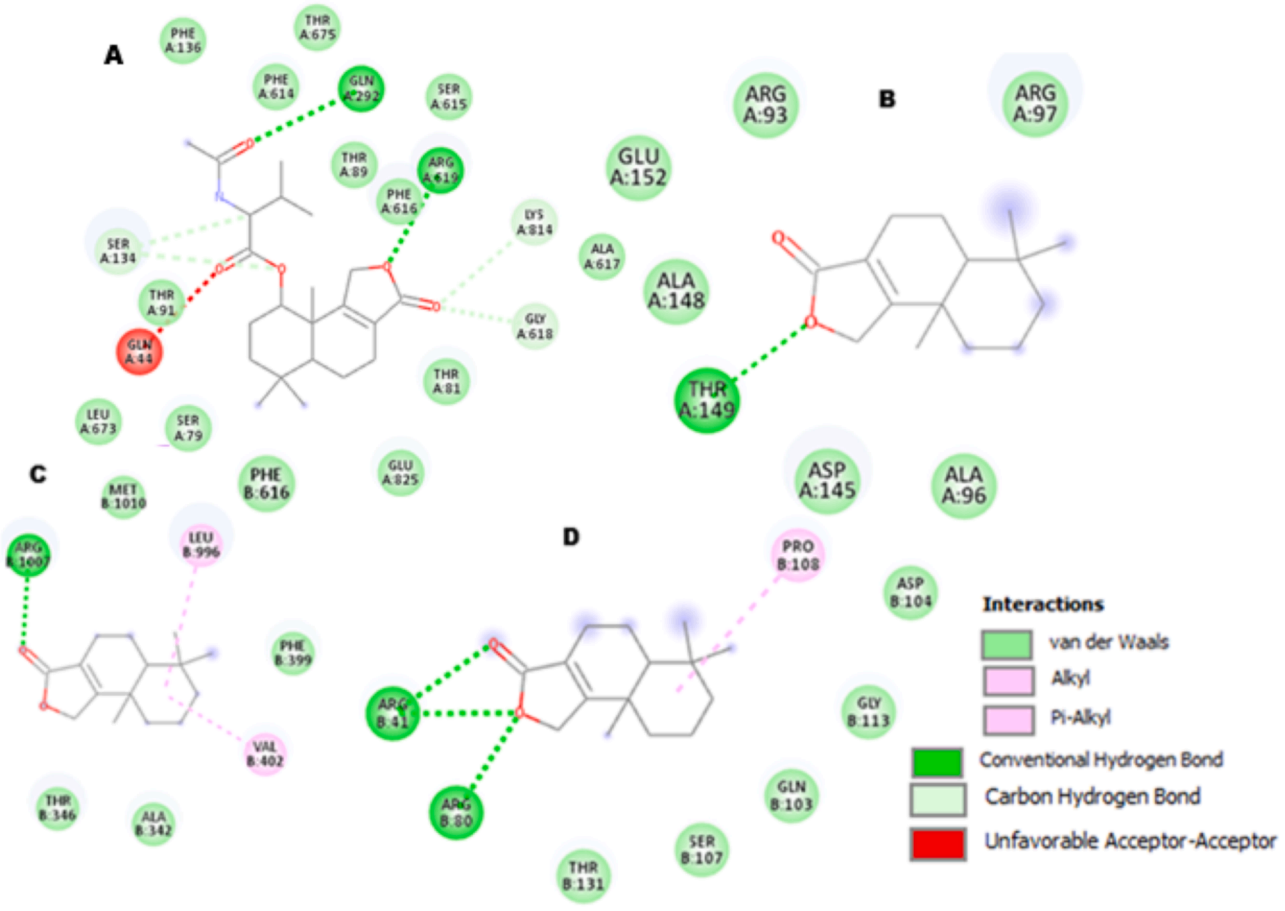

Fig. 3a. Hydrogen bonds and hydrophobic interaction of Purpuride with contact residues of *Burkholderia pseudomallei* (A) Multidrug efflux transporter BpeB (B) BipD of B. *pseudomallei* (C) Multidrug efflux transporter BpeF, and (D) Outer membrane porin (BpsOmp38).

3.4.2. Interaction of Purpuride with Burkholderia cepacia virulence and drug resistance proteins

Similar to the interaction of Purpuride with *Burkholderia pseudomallei* VDRP, the molecular docking study revealed the interaction of Purpuride with *Burkholderia cepacia* VDRP. The molecular docking score revealed that Purpuride had the highest binding affinity of −7.5 kcal·mol^{-1} with BceF Tyrosine Kinase Domain protein, −5.8 kcal·mol^{-1} Peptidoglycan-associated lipoprotein, −6.6 kcal·mol^{-1} Beta-lactamase, and −5.9 kcal·mol^{-1} with Dihydropteroate synthase (folP), respectively, Table 4b.

The interactions observed between the ligand and the receptors showed that Purpuride also formed a conventional hydrogen bond with amino acid ASP36, ARG47, SER94, TYR126, ARG220, and a pi-sigma bond with PHE95 at the active site of BceF Tyrosine Kinase Domain protein chain A. In addition, Purpuride interacted with ARG64 and VAL167 at the active site of Peptidoglycan-associated lipoprotein chain A with an alkyl bond. Furthermore, at the active site of the Beta-lactamase chain A, conventional hydrogen bonds were formed with ILE221 and ALA222. In contrast, no interaction was observed at the active site of Dihydropteroate synthase (folP) protein Fig. 3b. The coordinates of *Burkholderia cepacia* VDRP interaction with Purpuride are shown in **Table A.4b**.

The strong binding affinity of the ligand to *Burkholderia cepacia* VDRP in this study may be due to Purpuride forming a conventional hydrogen bond and an alkyl bond with the amino acids at the active sites of the *Burkholderia cepacia* VDRP, which may prevent amino acid expression, making it a promising inhibitor of *Burkholderia cepacia* VDRP. The result of this study also corresponds to the report of [53] who reported that TP1 demonstrated a strong interaction to the common peptide or inhibitor binding targets for lipopolysaccharide of *Escherichia coli*, with a binding affinity of −5.4 kcal·mol^{-1}, −8.1 kcal·mol^{-1} for autolysin, pneumolysin −7.7 kcal·mol^{-1}, and pneumococcal surface protein A (PspA) −7.3 kcal·mol^{-1} of *Streptococcus pneumoniae*. After a thorough review of literature, this study will be the first to report the *in-silico* activities of Purpuride from *Talaromyces marneffei* on BVDRP.

Table 4b
Binding affinity of Purpuride with *Burkholderia cepacia* VDRP.

Burkholderia cepacia complex		
Ligand	Targets	Binding Affinity (kcal·mol^{-1})
Purpuride	Beta-lactamase	−6.6
	Peptidoglycan-associated lipoprotein	−5.8
	Dihydropteroate synthase (folP)	−5.9
	BceF Tyrosine Kinase Domain	−7.5

Key: kcal·mol^{-1}- Kilocalorie per mole.

3.4.3. Comparison of binding affinity and interactions of Purpuride with reference inhibitors

The comparison of Purpuride and positive control inhibitor with *Burkholderia pseudomallei* Multidrug efflux transporter BpeB protein (responsible for efflux of drugs in *B. pseudomallei*) revealed that Purpuride localized to a distinct cavity (3716 Å^3) and demonstrated a stronger predicted affinity (−8.5 kcal·mol^{-1}), whereas 1-(1-Naphthylmethyl)piperazine, which was used as a reference inhibitor, bound to a large cavity (7758 Å^3) with a docking score of −7.9 kcal·mol^{-1} with *Burkholderia pseudomallei* Multidrug efflux transporter BpeB protein Table 5a.

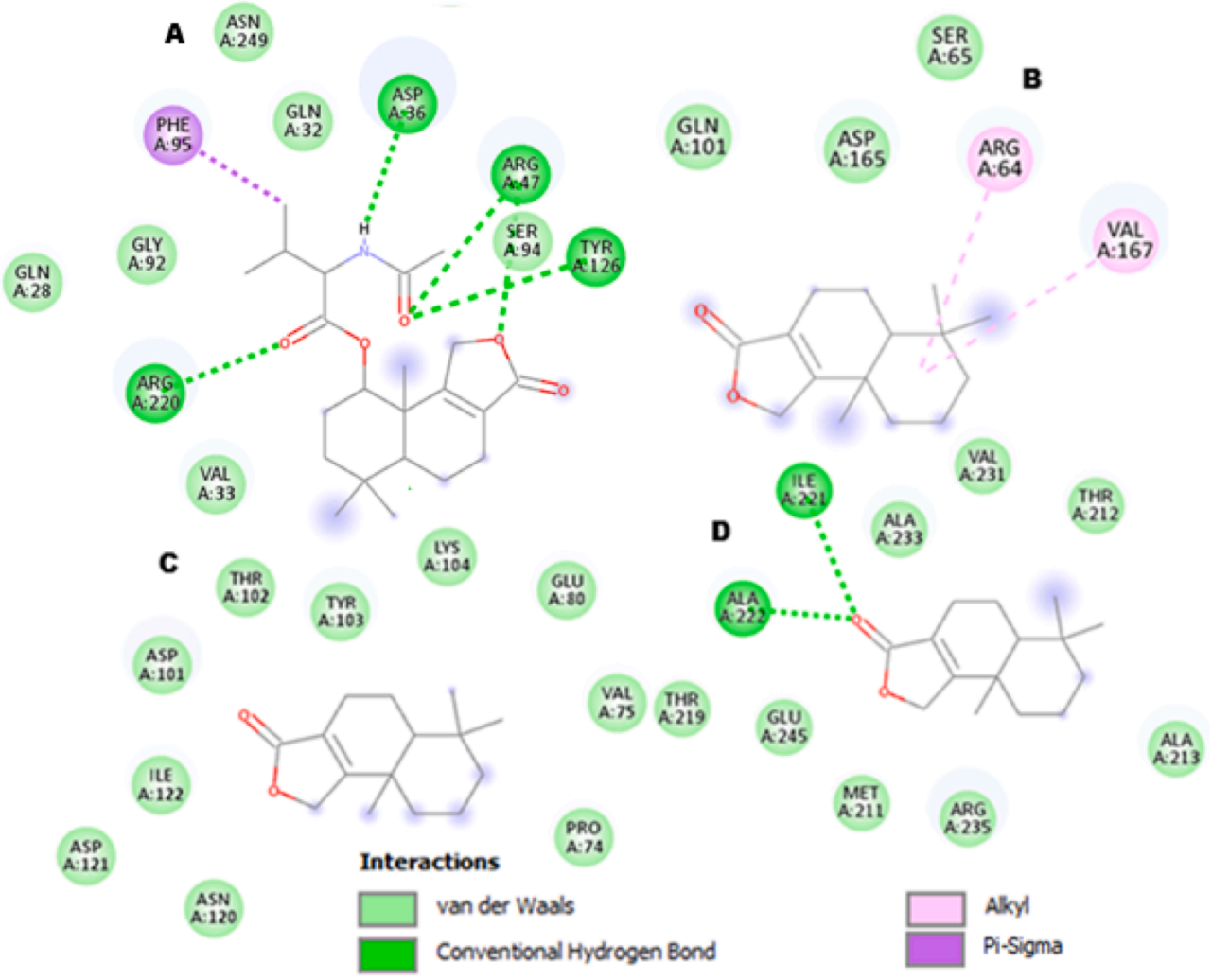

Fig. 3b. Hydrogen bonds and hydrophobic interaction of Purpuride with contact residues of *Burkholderia cepacia* (A) BceF Tyrosine Kinase Domain (B) Peptidoglycan-associated lipoprotein (C) Dihydropteroate synthase (folP) and (D) Beta-lactamase.

Table 5a
Docking scores and hydrogen bonds/hydrophobic interactions identified in the protein–ligand complexes of *Burkholderia pseudomallei* drug resistance protein.

Protein Targets (PDB IDs)	PubChem IDs and Name	Docking Score (kcal·mol^{-1})	Hydrogen Bonds/ Hydrophobic Interactions
7WLS	701891: 1-(1-Naphthylmethyl) piperazine	**−7.9**	ALA33, ALA299, ASN296, GLN34, GLU672, ILE670, PRO36, and VAL333
	101316833: Purpuride	**−8.5**	ARG619, GLN44, GLN292, GLY618, LYS814, and SER134

Key: 7WLS- Multidrug efflux transporter BpeB protein.

In addition, Purpuride interacted and formed a conventional hydrogen bond with amino acids ARG619 and GLN292, a carbon hydrogen bond with SER134, GLY618, and LYS814, and an unfavorable acceptor-acceptor bond with GLN44 at the active site of the receptor, whereas the 1-(1-Naphthylmethyl)piperazine interacted with the same amino acids ALA33, ALA299, VAL333, and ILE670 with a pi-alkyl bond. In addition, a carbon hydrogen bond and a pi-donor hydrogen bond were formed with GLN34 and PRO36, likewise a pi-anion with GLU672, a conventional hydrogen bond with ASN296 at the active site of receptor Fig. 4a. The coordinates of the inhibitors and *Burkholderia pseudomallei* drug resistance protein are shown in **Table A.5a.**

The extensive polar and hydrophobic contacts formed by Purpuride are consistent with its enhanced binding score relative to the control. The formation of these bonds and the interactions with amino acids at the active site of the receptor, demonstrated by Purpuride and the reference inhibitor, indicated that these inhibitors may prevent the expression of this protein in *Burkholderia* sp. The result of this study revealed that Purpuride from *Talaromyces marneffei* strain SA2a could serve as a potential inhibitor of the Multidrug efflux transporter BpeB protein in *Burkholderia pseudomallei*.

The result of this study is similar to the findings of [54], who evaluated the performance of an efflux pump inhibition assay in comparison with RT-qPCR, to assess efflux pump overexpression in sixty MDR clinical *A. baumannii* strains. In their findings, 1-(1-NaphthylMethyl)-Piperazine (NMP) inhibited efflux pump expression in 34 strains of *A. baumannii* and was negative in 27 strains. This is in agreement with our study that 1-(1-NaphthylMethyl)-Piperazine (NMP) and Purpuride interacted with amino acids at the active sites of *Burkholderia pseudomallei* Multidrug efflux transporter BpeB protein chain A. This report provides baseline *in silico* molecular prediction data that Purpuride could be used as a potential inhibitor of efflux pumps in Gram-negative bacteria.

Purpuride and reference inhibitor Luteolin demonstrated a good binding affinity with *Burkholderia cepacia* BceF Tyrosine Kinase Domain

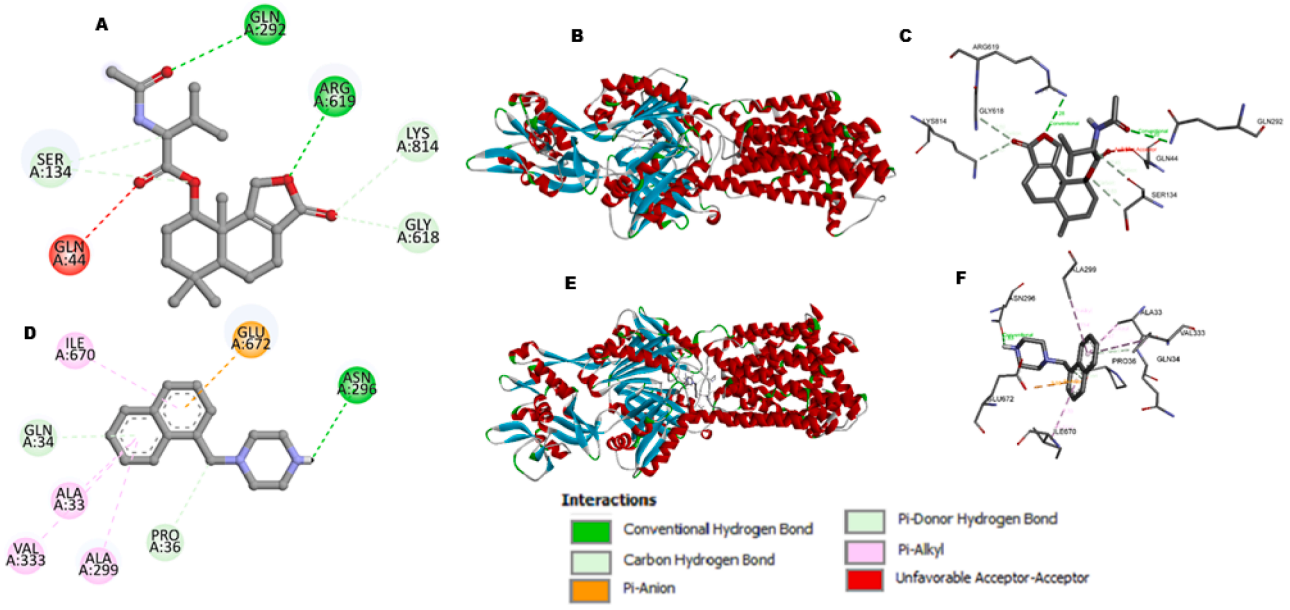

Fig. 4a. (A&D) 2D hydrogen bonds and hydrophobic interaction of Purpuride and 1-(1-Naphthylmethyl)piperazine with contact residues of *Burkholderia pseudomallei* Multidrug efflux transporter BpeB protein indicating ligand stabilization within the binding pocket (B&E) 3D representation of Purpuride and 1-(1-Naphthylmethyl)piperazine with residues showing ligand orientation within the binding pocket (C&F) 3D Interaction of Purpuride and 1-(1-Naphthylmethyl)piperazine with binding pocket.

protein (responsible for biofilm formation in *B. cepacia*). Luteolin docked within a 387 Å^3 cavity and achieved a binding score of −8.0 kcal·mol^{-1}, whereas Purpuride occupied the same pocket but showed a slightly weaker score (−7.5 kcal·mol^{-1}) Table 5b.

Purpuride interacted with amino acids present at the active sites of the *Burkholderia cepacia* BceF Tyrosine Kinase Domain protein chain A by forming conventional hydrogen bonds with ASP36, ARG47, TYR126, ARG220, and a pi-sigma bond with PHE95. Furthermore, Luteolin interacted and formed a conventional hydrogen bond with ASP36, ARG47, TYR126, ASN249, a pi-pi stacked with PHE95, an unfavourable acceptor-acceptor with ARG220, and an attractive charge, pi-cation, and pi-anion with ASP36 at the active site of the *Burkholderia cepacia* BceF Tyrosine Kinase Domain protein chain A Fig. 4b. The coordinates of the inhibitors and *Burkholderia cepacia* biofilm formation protein are shown in **Table A.5b**, and docking scores and contact residues identified in the protein–ligand complexes are shown in **Table A.5c&d.**

These interactions with the amino acids at the active site of the receptor with the respective bonds indicate the potential of the inhibitor to prevent the expression of *Burkholderia cepacia* BceF Tyrosine Kinase Domain protein. The interaction observed between Purpuride and the amino acids at the active site of the *Burkholderia cepacia* BceF Tyrosine Kinase Domain protein chain A revealed that Purpuride could serve as a potential inhibitor of this protein, as there were no established specific inhibitors of this *Burkholderia cepacia* BceF Tyrosine Kinase Domain protein previously reported. However, the results of this study indicate that Luteolin, which served as a reference ligand, forms a broader network of stabilizing contacts than Purpuride, suggesting a stronger affinity and a potential inhibitor of 6Z09.

According to [55], Luteolin acts as a novel HGF/c-Met inhibitor by suppressing phosphorylation of c-Met tyrosine kinase, induced by HGF, thereby inhibiting cancer cell invasion. Luteolin reduces the expression of VEGF mRNA by inhibiting NF-κB transcription activity, thus inhibiting VEGF secretion. Furthermore, in bacterial cells, Luteolin interferes with kinase-mediated pathways to inhibit bacterial growth and also downregulates tyrosine kinase signaling genes. In addition, research has demonstrated that Luteolin can act on serine/threonine phosphatase (STP) and serine/threonine kinase (PknB) enzymes to disrupt signaling and growth in drug-resistant *Trueperella pyogenes* [36].

Across both proteins, Purpuride displayed competitive binding relative to reference 1-(1-Naphthylmethyl)piperazine. Meanwhile, on 6Z0P, Luteolin retained the stronger predicted affinity, whereas on 7WLS, Purpuride surpassed the positive control. These findings highlight Purpuride as a versatile scaffold with potential binding promiscuity across distinct protein pockets and as a stronger inhibitor of 7WLS than reference 1-(1-Naphthylmethyl)piperazine.

Table 5b
Docking scores and hydrogen bonds/hydrophobic interactions identified in the protein–ligand complexes of *Burkholderia cepacia* biofilm formation protein.

Protein Targets (PDB IDs)	PubChem IDs and Name	Docking Score (kcal·mol^{-1})	Hydrogen Bonds/ Hydrophobic Interactions
6Z0P	5280445: Luteolin	**−8.0**	ARG47, ARG220, ASP36, ASN249, PHE95, and TYR126
	101316833: Purpuride	**−7.5**	ARG47, ARG220, ASP36, PHE95, and TYR126

Key: 6Z0P- BceF Tyrosine Kinase Domain.

3.5. *Molecular dynamics simulation of ligands with Burkholderia virulence and drug-resistance proteins*

3.5.1. *Molecular dynamics simulation*

The molecular dynamics simulation 100-ns revealed the structural stability of BceF tyrosine kinase domain complexed with Luteolin and Purpuride, as well as Multidrug efflux transporter BpeB complexed with 1-(1-Naphthylmethyl)piperazine and Purpuride.

3.5.1.1. *Root-mean-square deviation (RMSD)*

3.5.1.1.1. Stability of BceF tyrosine kinase domain in complex with ligands. Structural stability and global drift (Fig. 5a) Luteolin–6Z0P displayed a stable trajectory mean backbone RMSD = 0.502 ± 0.278 nm (SD), median 0.283 nm, minimum 0.125 nm, and maximum 1.077 nm (SEM = 0.00278). These values indicate that the complex equilibrated rapidly and remained near a single conformational basin for the majority of the run. In contrast, Purpuride–6Z0P complex showed a

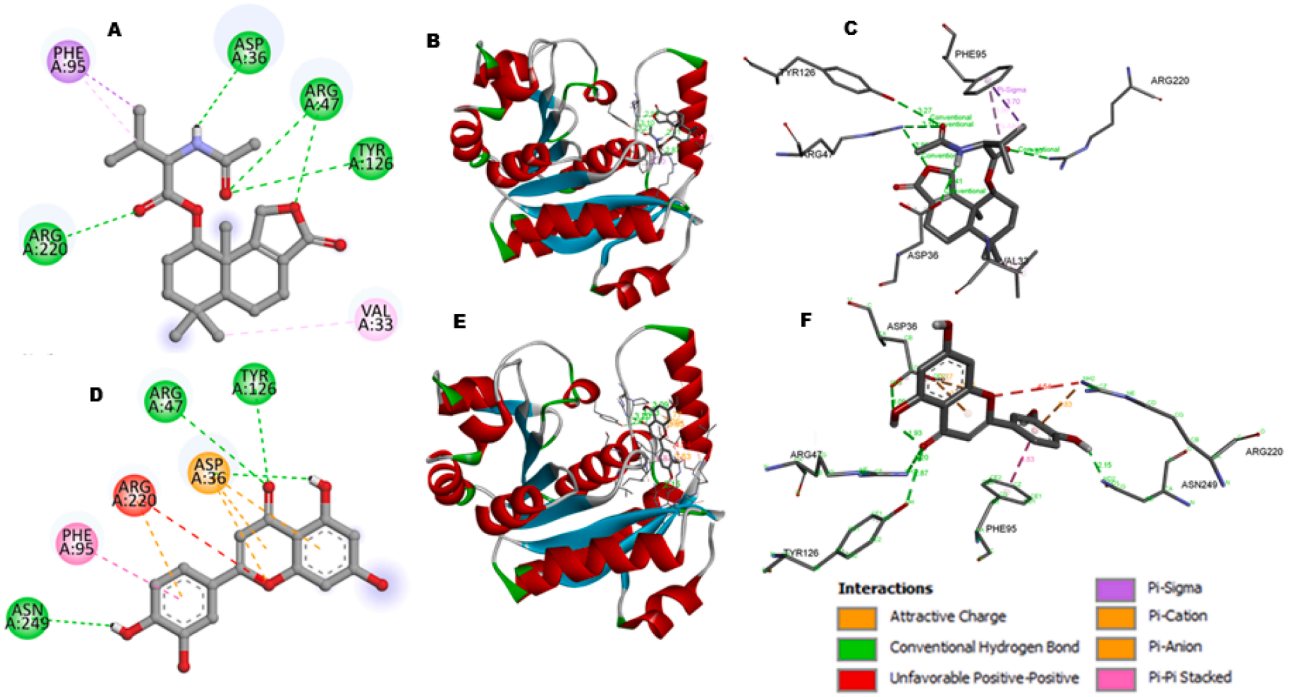

Fig. 4b. (A&D) 2D hydrogen bonds and hydrophobic interaction of Purpuride and Luteolin with contact residues of *Burkholderia cepacia* BceF Tyrosine Kinase Domain protein, indicating ligand stabilization within the binding pocket (B&E) 3D representation of Purpuride and Luteolin with residues showing ligand orientation within the binding pocket (C&F) 3D Interaction of Purpuride and Luteolin with binding pockets.

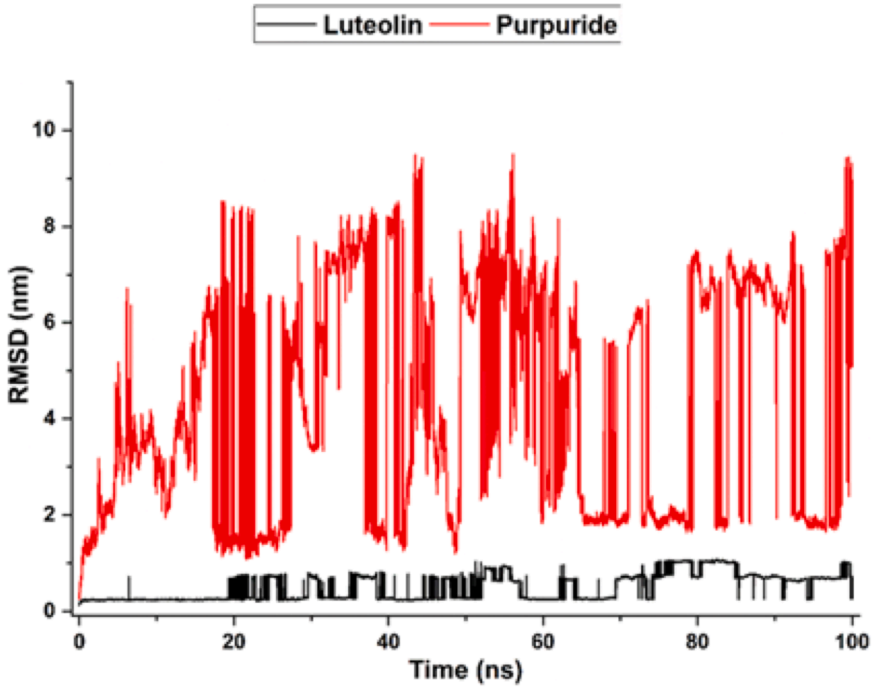

Fig. 5a. RMSD profiles of Luteolin–6Z0P (black) and Purpuride–6Z0P (red) over 100 ns. The Luteolin–6Z0P complex (black) shows minimal deviation (~0.5 nm), indicating strong structural stability, while Purpuride–6Z0P (red) displays large fluctuations up to 9.5 nm, reflecting significant conformational drift or partial ligand dissociation.

dramatic departure from this behaviour with a mean RMSD = 4.275 ± 2.378 nm, a median of 3.680 nm, and an extreme maximum RMSD of 9.50 nm (SEM = 0.02378).

The very large mean and maximum RMSD for Purpuride indicate one or more major structural rearrangements during the trajectory, most likely due to ligand displacement domain movement rather than simple local fluctuations. Visual inspection of the trajectory frames is recommended to identify the timing and nature of these events. Additionally, Luteolin maintains a compact and stable complex with the kinase domain across 100 ns. The generated PDB snapshots, taken at 10 ns intervals, are shown in **Fig. A1.** The extremely high RMSD of Purpuride complex strongly suggests loss of a native binding mode (partial/

complete unbinding or large conformational drift), consistent with the low average number of hydrogen bonds observed for Purpuride in this system (see H-bond section). Together, RMSD and H-bond data indicate that Luteolin is the superior binder for 6Z0P under these simulation conditions.

3.5.1.1.2. Stability of multidrug efflux transporter BpeB protein in complex with ligands. The 1-(1-Naphthylmethyl)piperazine and Purpuride in complex with 7WLS show low and comparable RMSD behaviour in the BpeB system: 1-(1-Naphthylmethyl)piperazine mean RMSD = 0.443 ± 0.069 nm (median 0.440 nm, max 0.630 nm), and Purpuride mean RMSD = 0.453 ± 0.090 nm (median 0.457 nm, max 1.061 nm). The slightly higher SD and occasional peaks for Purpuride reflect transient rearrangements rather than sustained unbinding **Table A.6**. Overall, both complexes remain within a single conformational ensemble for the majority of the simulation.

Purpuride is dynamically well accommodated by 7WLS; its RMSD profile is essentially indistinguishable from the reference ligand, indicating stable binding over 100 ns Fig. 5b. The transient excursions (peaks near 1.0 nm) likely represent side-chain reorganizations or local loop motions rather than wholesale dissociation.

The results of this study are similar to the RMSD analysis conducted by [56] to understand the structural stability of 5A5F–9,10-Anthracenedione and 1DNU–9,10-Anthracenedione, as well as 5A5F–Amoxicillin and 1DNU–Ascorbic Acid complexes over a 100 ns MD simulation. In their study, 5A5F–Amoxicillin complex displayed a more stable profile, with RMSD values decreasing at 100 ns and fluctuating consistently within the range of 1.5–2 Å, and 1DNU–Ascorbic Acid complex exhibited an even more stable profile, with RMSD values ranging from 1.71 Å. Likewise, [57] evaluated MD simulations 100-ns of Oleandrin with Prostaglandin-endoperoxide synthase 2 (PTGS2) and Mitogen-Activated Protein Kinase 1 (MAPK1). The RMSD analysis demonstrated minor fluctuations, stabilizing after 20 ns, confirming the structural integrity of the complexes.

3.5.1.1.3. Center of mass (CoM) analysis. The center of mass (CoM) analysis was performed to evaluate the positional stability of Luteolin and Purpuride within the BceF tyrosine kinase domain over 100 ns of molecular dynamics simulation. The Luteolin–BceF complex exhibited a consistent CoM distance with an average of 0.76 ± 0.05 nm, indicating that the ligand remained tightly bound within the active site Fig. 6 & **Table A.7.** In contrast, the Purpuride–BceF complex showed a significantly higher average CoM distance of 2.23 ± 1.00 nm, with large fluctuations throughout the simulation, suggesting a loss of stable interaction and partial displacement from the binding pocket.

3.5.1.2. Radius of gyration (Rg, nm)

3.5.1.2.1. BceF tyrosine kinase domain in complex with ligands. Mean Rg for the Luteolin complex = 1.7542 ± 0.0069 nm (range 1.728–1.780 nm), and for Purpuride = 1.7585 ± 0.0074 nm (range 1.728–1.794 nm). The two trajectories maintain nearly identical global compactness, with Purpuride exhibiting a very slight upward shift (Δmean ≈ 0.0044 nm) and marginally larger spread. Despite the large RMSD observed for Purpuride, the similarity in mean Rg indicates that the core fold of the protein remains largely intact for much of the trajectory; the large RMSD likely arises from localized or domain/loop excursions rather than wholesale collapse or expansion of the fold Fig. 7.

3.5.1.2.2. Multidrug efflux transporter BpeB protein in complex with ligands. Mean Rg for the 1-(1-naphthylmethyl)piperazine = 3.6816 ± 0.0310 nm, and for Purpuride = 3.6841 ± 0.0262 nm. The differences are negligible (Δmean ≈ 0.0025 nm), indicating preserved tertiary structure and no global unfolding in either complex. Both complexes retain tight structural integrity; Rg supports the conclusion from RMSD that Purpuride is stably bound to 7WLS without inducing global expansion or collapse Fig. 7.

3.5.1.3. Solvent accessible surface area (SASA, nm²)

3.5.1.3.1. BceF tyrosine kinase domain in complex with ligands. Mean SASA (system) with Luteolin = 119.572 ± 2.008 nm², with Purpuride = 119.960 ± 1.879 nm². The difference is small (~0.39 nm²) and within one standard deviation, indicating essentially unchanged solvent exposure between the two complexes over the production period Fig. 8. Because SASA is nearly identical, the large RMSD for Purpuride trajectory likely reflects local rearrangements rather than a net increase in exposed surface area, consistent with a scenario where the ligand relocates to a different pocket or a flexible loop reorients without globally exposing the protein.

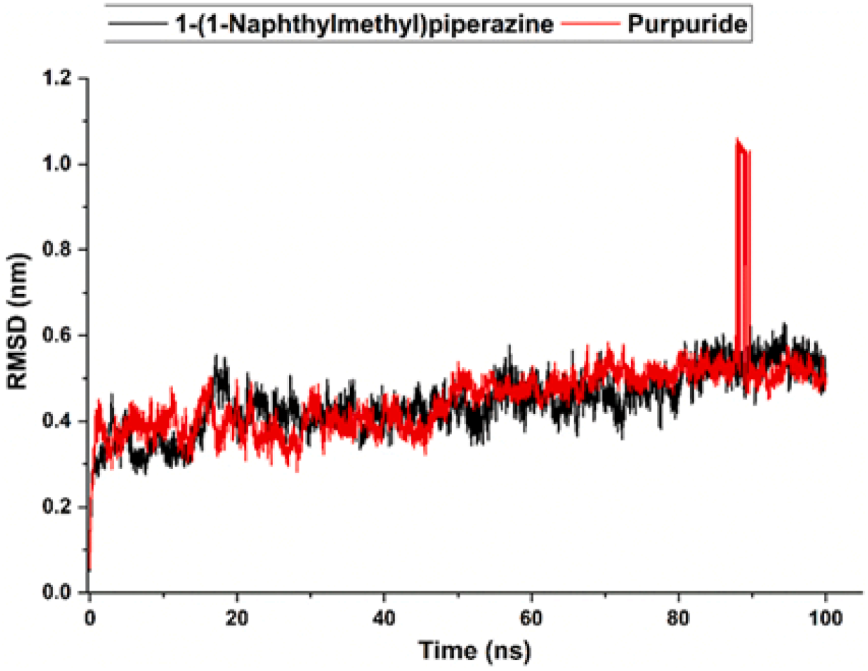

Fig. 5b. RMSD profiles of 1-(1-naphthylmethyl)piperazine–7WLS (black) and Purpuride–7WLS (red). Both the reference ligand (black) and Purpuride (red) remain stable (~0.45 nm), indicating that Purpuride achieves comparable binding stability and structural maintenance to the reference ligand within 7WLS.

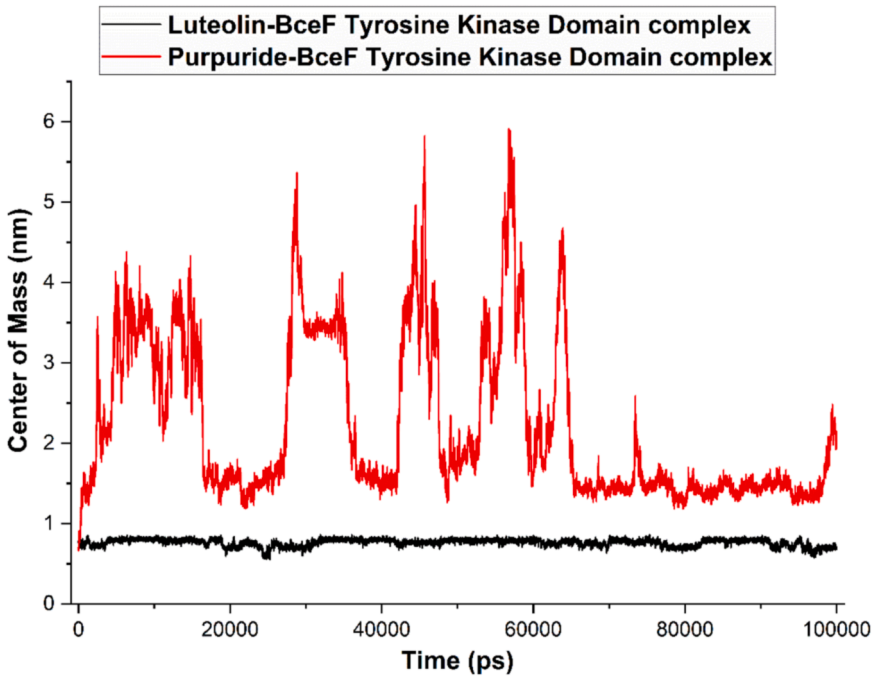

Fig. 6. Center of Mass (CoM) analysis of the Luteolin– and Purpuride–BceF tyrosine kinase domain complexes throughout the 100 ns MD simulation. The CoM displacement of Luteolin remains stable around 0.76 nm, indicating a tightly bound conformation within the active site, whereas Purpuride shows pronounced fluctuations with an average of 2.23 nm, reflecting reduced stability and partial ligand dissociation.

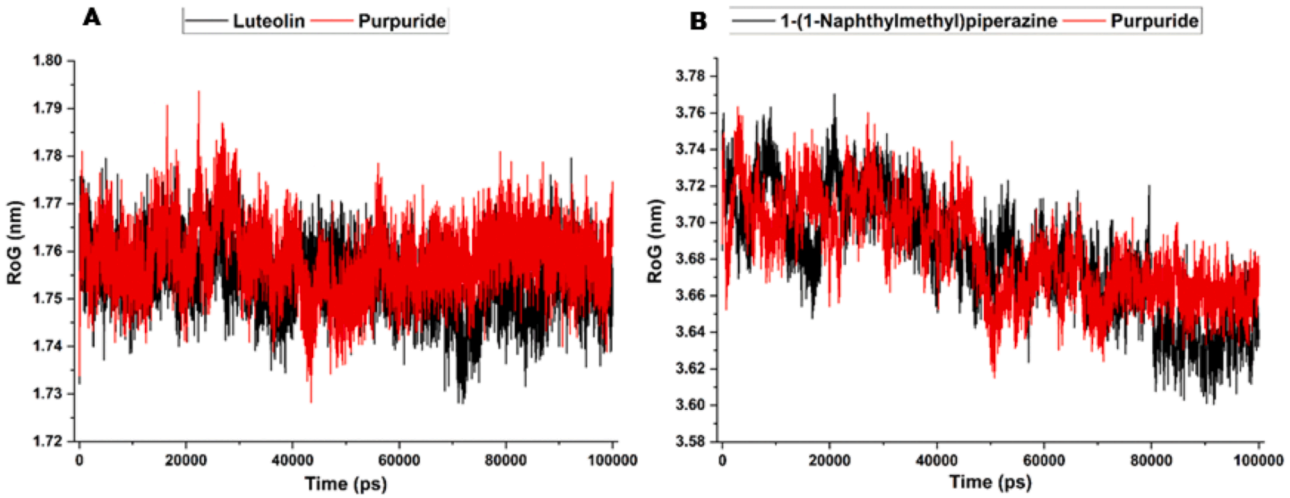

Fig. 7. Radius of gyration (Rg) profiles for protein complexes over 100 ns (A) Comparison of Luteolin–6Z0P and Purpuride–6Z0P, both maintaining ~1.75 nm Rg, indicates that both maintain compact protein conformations. Despite the high RMSD in Purpuride, the consistent Rg suggests that the overall protein fold remains stable (B) 1-(1-naphthylmethyl)piperazine –7WLS and Purpuride–7WLS, both with a value of ~3.68 nm, confirming that Purpuride binding does not induce significant conformational expansion or collapse in 7WLS.

3.5.1.3.2. Multidrug efflux transporter BpeB protein in complex with ligands. Mean SASA for 1-(1-naphthylmethyl)piperazine = 456.324 ± 5.458 nm^2, for Purpuride = 451.831 ± 5.507 nm^2. Purpuride complex shows a modest reduction in SASA (~4.5 nm^2), consistent with a slightly more buried or compact local binding mode Fig. 8. The decreased SASA for Purpuride suggests it occupies a pocket that is slightly more occluded or that Purpuride induces local packing that reduces solvent exposure of surface residues, an effect that correlates with the greater average number of hydrogen bonds observed for Purpuride in this system.

Similar to this study, [58] conducted Solvent Accessible Surface Area (SASA) and Polar Surface Area (PSA) analyses on protein targets implicated in diabetes (PTK2 (3PXK) and α-Amylase (3BAJ)) in complex with quercetin. In their findings, they observed minor SASA variations and consistent PSA values in the 3PXK and 3BAJ systems, which reflect transient conformational adjustments and sustained polar interactions, as well as minimal disruption of the binding environment.

3.5.1.4. Hydrogen bonding (occupancy and dynamics)

3.5.1.4.1. BceF tyrosine kinase domain in complex with ligands. Average number of ligand–protein hydrogen bonds: Luteolin = 0.918 ± 0.817, Purpuride = 0.127 ± 0.376 (max observed H-bonds: Luteolin 4, Purpuride 3) **Table A.8**. Luteolin forms hydrogen bonds with the binding site more persistently; Purpuride shows almost no persistent H-bonding. Persistent hydrogen bonds are a hallmark of stable binding in this pocket; Luteolin's near-one average H-bond (with frequent events of 1–2 H-bonds) supports its low RMSD and stable binding. Purpuride's

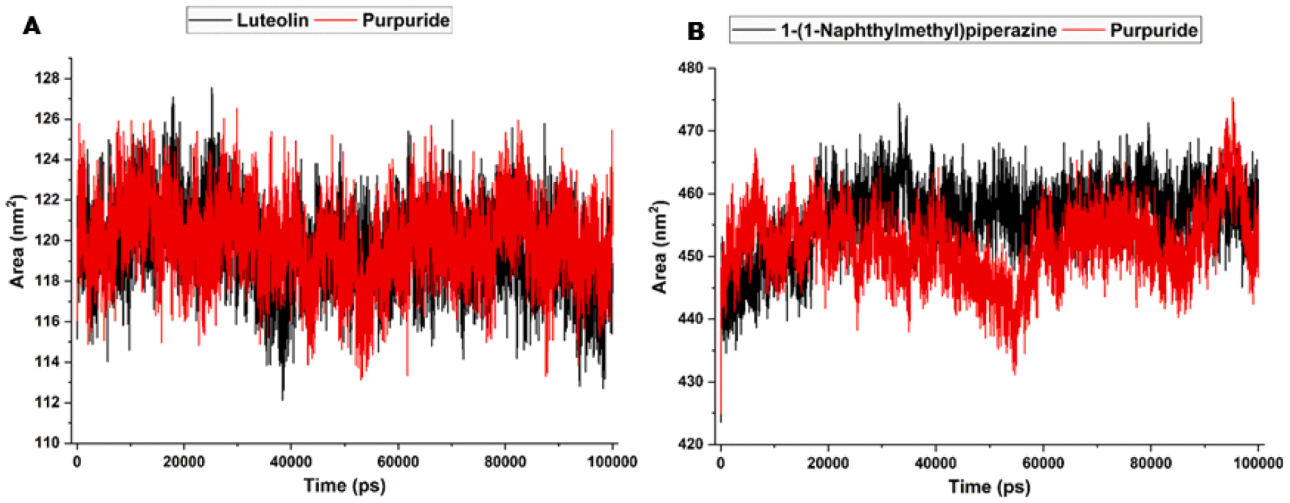

Fig. 8. (A) SASA of Luteolin–6Z0P and Purpuride–6Z0P, nearly identical (~120 nm^2), indicating that Purpuride binding does not significantly alter overall solvent exposure of the protein (B) SASA of 1-(1-naphthylmethyl)piperazine–7WLS and Purpuride–7WLS. Purpuride shows slightly reduced SASA (~451.8 nm^2 vs. 456.3 nm^2), suggesting Purpuride adopts a more buried and tightly packed binding mode.

near-zero average indicates weak polar anchoring and helps explain the dramatic RMSD excursions (probable unbinding or relocation) Fig. 9.

3.5.1.4.2. Multidrug efflux transporter BpeB protein in complex with ligands. Average number of ligand–protein hydrogen bonds: 1-(1-Naphthylmethyl)piperazine = 0.357 ± 0.496, Purpuride = 0.935 ± 1.020 (Purpuride observed up to 8 H-bonds in snapshots) **Table A.8**. Purpuride forms substantially more hydrogen bonds on average in the BpeB binding environment. Higher H-bond occupancy for Purpuride correlates with its lower SASA and stable RMSD in 7WLS together, these metrics indicate a binding mode with both polar anchoring and close packing, consistent with a higher predicted affinity from docking and with the observed dynamic stability Fig. 9.

The number of hydrogen bonds formed in this study corresponds to the study of [56], which evaluated binding stability and hydrogen bonding patterns with a maximum of 8 hydrogen bonds in 5A5F–Amoxicillin complex, a maximum of 5 hydrogen bonds in 5A5F–9,10 Anthracenedione complex, and 3 hydrogen bonds in 1DNU–9,10- Anthracenedione complex recorded.

3.5.1.5. Root-mean-square fluctuation (RMSF, per-residue flexibility)

3.5.1.5.1. BceF tyrosine kinase domain in complex with ligands. Mean RMSF (all residues) is 0.149 ± 0.301 nm for Luteolin and 0.109 ± 0.0499 nm for Purpuride. The RMSF distributions show that most residues are relatively rigid (median values ~0.07–0.28 nm), but Luteolin's trajectory contains outlier(s) with very large local fluctuations (reported maximum RMSF up to 4.80 nm), indicating one or a few residues/regions undergo exceptional mobility (likely flexible termini or a loop). The two RMSF distributions are statistically different (two-sample test, $p \approx 0.0407$), and the residue-by-residue correlation between the two simulations is low ($r \approx 0.197$), implying that Purpuride and Luteolin induce different local mobility signatures in 6Z0P. Although the global RMSF mean is slightly lower for Purpuride Fig. 10, the extremely high RMSD observed for Purpuride combined with an RMSF pattern that differs from Luteolin suggests that Purpuride sampling includes episodes that change which residues are mobile (e.g., a loop becoming highly flexible when the ligand dissociates). The significant p-value and low correlation indicate nontrivial differences in local dynamics induced by each ligand.

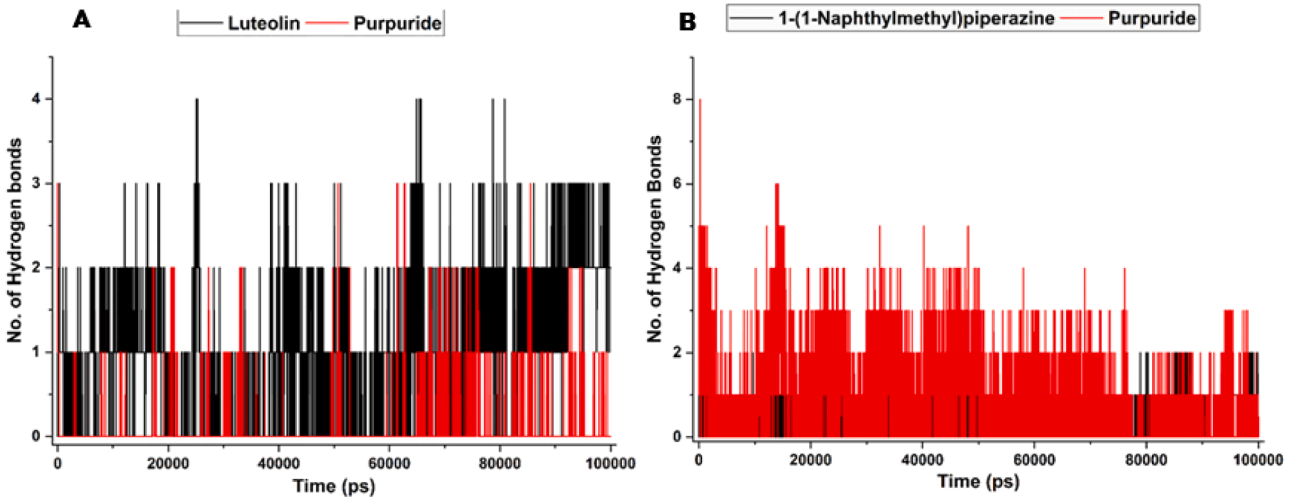

Fig. 9. (A) Hydrogen bond dynamics for 6Z0P complexes over 100 ns. Luteolin–6Z0P (black) maintains an average of ~1 hydrogen bond throughout the trajectory, while Purpuride–6Z0P (red) forms few or transient H-bonds, indicating weaker polar stabilization and reduced binding persistence (B) Hydrogen Bonds. In 7WLS, 1-(1-Naphthylmethyl)piperazine forms ~0.36 H-bonds on average, while Purpuride (red) forms nearly one hydrogen bond (~0.94), with transient peaks up to eight H-bonds, indicating enhanced polar stabilization and tight binding.

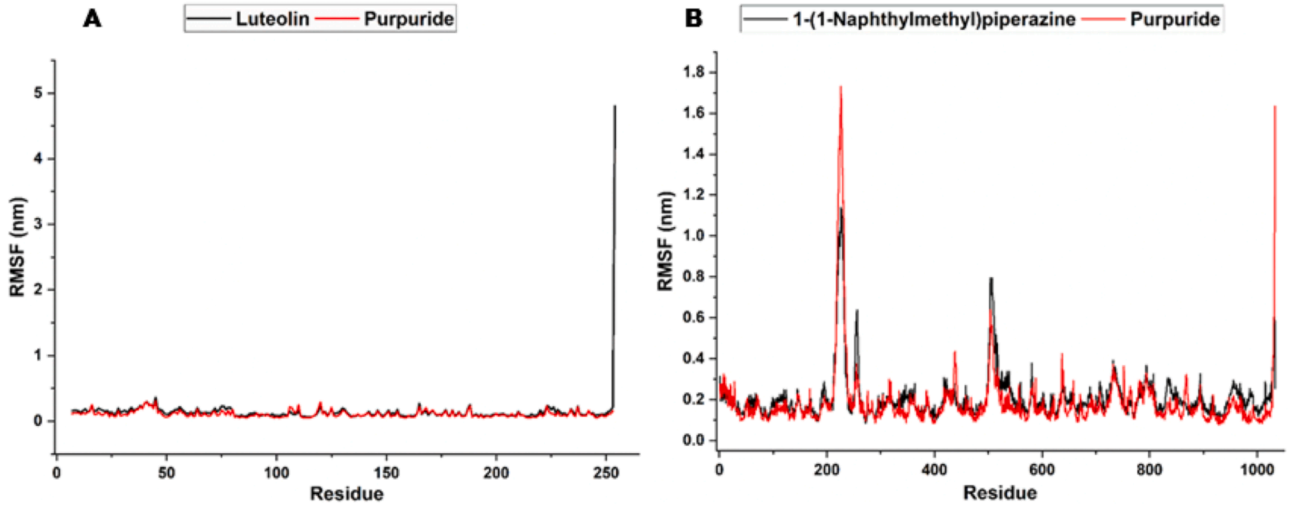

Fig. 10. Root Mean Square Fluctuation (RMSF) per residue (A) Luteolin–6Z0P vs. Purpuride–6Z0P exhibit distinct local flexibility patterns. Purpuride induces higher mobility in certain loops, suggesting ligand-induced instability and local rearrangements consistent with its large RMSD (B) 1-(1-Naphthylmethyl)piperazine–7WLS vs. Purpuride–7WLS display similar RMSF profiles, with Purpuride slightly reducing loop flexibility at several positions. This indicates stable binding and minor local stabilization by Purpuride.

3.5.1.5.2. Multidrug efflux transporter BpeB protein in complex with ligands. Mean RMSF values are 0.210 ± 0.119 nm for 1-(1-Naphthylmethyl)piperazine and 0.189 ± 0.160 nm for Purpuride. RMSF peaks (max ~1.14 nm for the control; up to ~1.73 nm observed in Purpuride run) are concentrated in loop/turn regions. RMSF distributions are significantly different ($p \approx 0.00049$), but the per-residue RMSF correlation is high ($r \approx 0.873$) **(Table A.10)**, meaning the two simulations share a similar mobility pattern across residues, with Purpuride reducing fluctuation at several localized sites. The high correlation shows the backbone response of 7WLS to both ligands is broadly similar (same flexible regions), but the significant p-value and slightly lower mean RMSF for Purpuride suggest it stabilizes certain loop regions more effectively than the 1-(1-Naphthylmethyl)piperazine (Fig. 10) a result consistent with the higher H-bond occupancy and reduced SASA noted above.

Two-sample statistical comparisons of RMSF distributions produced $p \approx 0.0407$ for 6Z0P and $p \approx 0.00049$ for 7WLS, indicating significant per-residue mobility differences between ligand-bound simulations in both systems (more pronounced for 7WLS). The per-residue RMSF correlation between ligands is low for 6Z0P ($r \approx 0.197$), but high for 7WLS ($r \approx 0.873$), supporting the interpretation that Purpuride induces distinct dynamic behaviour in 6Z0P (including disruptive events) but acts similarly to the 1-(1-Naphthylmethyl)piperazine in 7WLS, with modest local stabilizing effects shown in **Table A.10**.

RMSF analysis provides insights into the flexibility of individual residues within protein-ligand complexes [56]. reported a higher stability of residues in 5A5F–Amoxicillin complex and an increased flexibility in specific residues of 1DNU–Ascorbic Acid complex. Similarly, [57] identified flexible regions, especially in loop areas, throughout the RMSF analysis of Oleandrin with PTGS2 and MAPK1.

3.5.1.6. Total energy analysis. The stability of the protein–ligand complexes was then assessed by considering total potential energy during the 100 ns MD trajectories Fig. 11. Energy traces were stable in all four systems, with no systematic drift in energy traces thus, the simulations were equilibrated at a total energy level and clearly demonstrated there

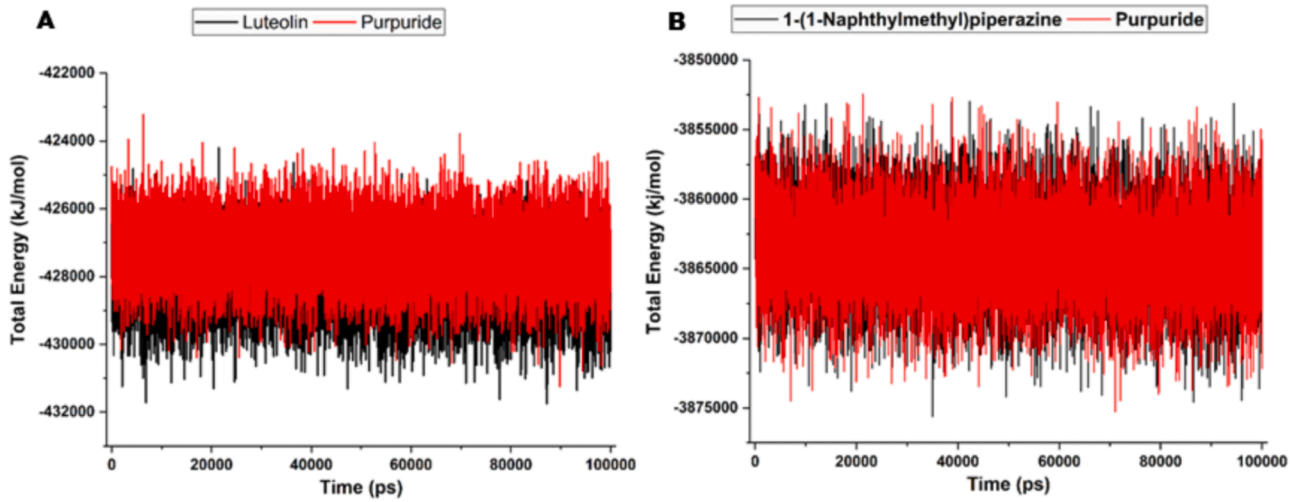

Fig. 11. (A) Total potential energy of 6Z0P complexes during 100 ns MD simulations. Luteolin–6Z0P (black) and Purpuride–6Z0P (red) show stable potential energy fluctuations (~−4.3 × 10^5 kJ/mol), confirming equilibrated systems with no artificial drift or instability (B) Total potential energy of 7WLS complexes during 100 ns MD simulations. Both the reference ligand–7WLS (black) and Purpuride–7WLS (red) complexes converge to similar energy levels (~−3.86 × 10^6 kJ/mol), confirming dynamic stability and energy equilibration.

were no artificial instabilities in MD time integration.

For the 6Z0P system, the total potential energy of the Luteolin complex was -4.28×10^5 kJ·mol^{-1} and the potential energy of Purpuride complex was -4.27×10^5 kJ·mol^{-1} ($\pm 1.2 \times 10^3$ kJ·mol^{-1} fluctuation). While the total potential energy was very comparable - and again tempered higher RMSD for Purpuride relative to Luteolin and weaker hydrogen bonding - these results indicated that energetically, both systems achieved dynamic stability throughout the trajectory. In system 7WLS, both complexes exhibited nearly identical energetics, -3.86×10^6 kJ·mol^{-1}, with even less variance in the basic data for 1-(1-naphthylmethyl)piperazine relative to Purpuride.

Similar energetics confirmed RMSD and Rg observations against time. In the same protein system, Purpuride achieves a comparable level of binding stability to reference ligand 1-(1-naphthylmethyl)piperazine. Total energies were summarized in **Table A.11** for each protein-ligand complex and reflected energetic comparability of reference and Purpuride complexes in 7WLS relative to the small degree of destabilization in 6Z0P. The binding free energy analysis provided strong energetic evidence for stability [58]. In a study by [59], the total binding energies between the ligands Cmpd1 and 15e and protein Ag3HKT were found to

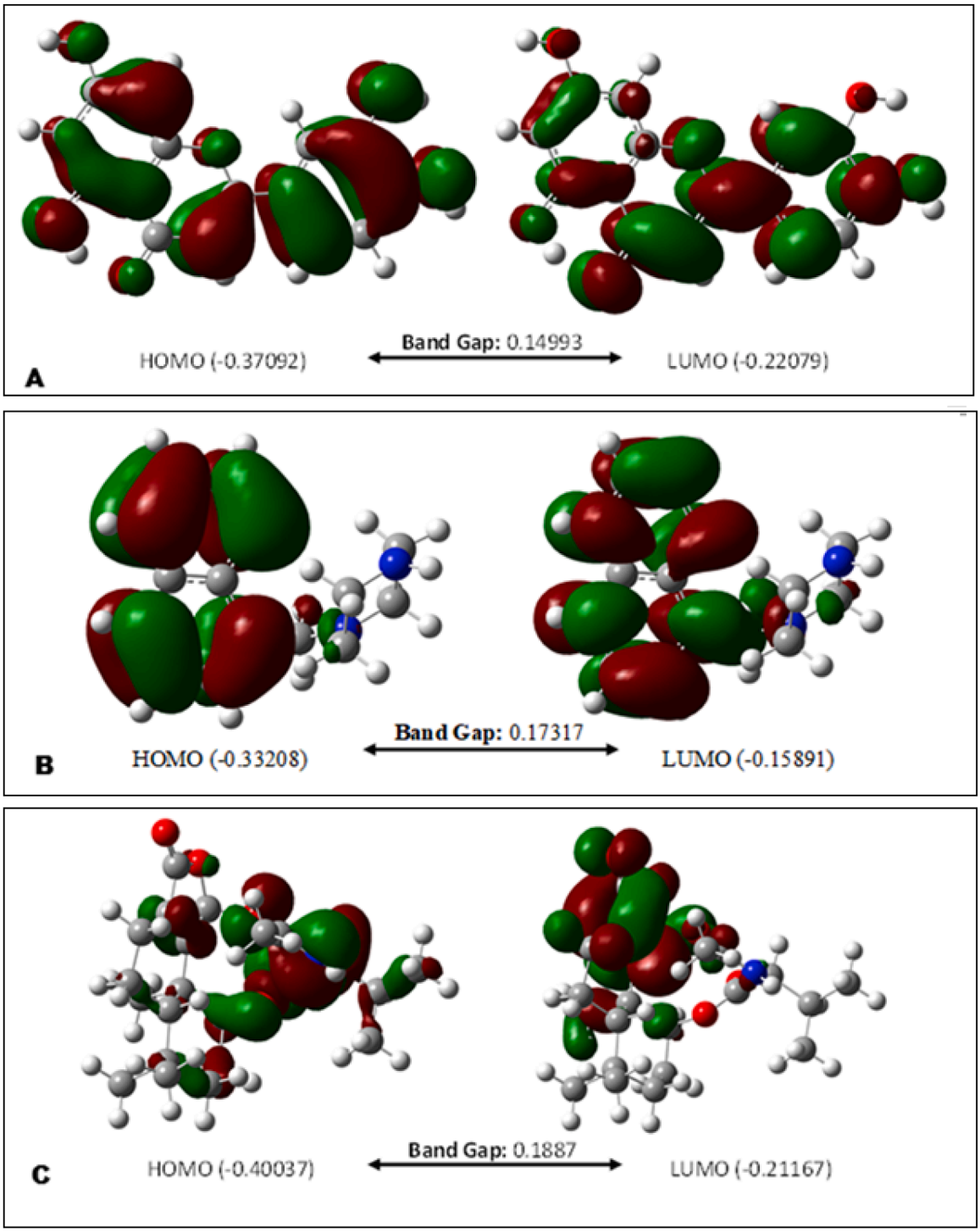

Fig. 12. Optimized 3D geometry and frontier orbital HOMO, and LUMO distribution of (A) Luteolin (B) of 1-(1-naphthylmethyl)piperazine (C) Purpuride produce the largest energy gap (0.1887 a.u.) among all ligands, indicating high kinetic stability and strong molecular rigidity, consistent with its stable binding in 7WLS.

be − 26.64 kcal·mol^{-1} and − 24.26 kcal·mol^{-1}, respectively. Additionally, [56] reported the most favourable binding energy (ΔGbind = −145.13 ± 13.11 kcal·mol^{-1}) in 1DNU–9,10-Anthracenedione complex and comparatively weaker interactions in the binding energy of 5A5F–9, 10-Anthracenedione (ΔGbind = −60.62 ± 4.66 kcal·mol^{-1}) and 5A5F–Amoxicillin (ΔGbind = −34.31 ± 7.94 kcal·mol^{-1}) complexes.

Overall, BceF Tyrosine Kinase Domain (6Z0P): These results (very large RMSD for Purpuride, very low H-bond occupancy, and changed RMSF pattern) suggest that Purpuride does not stably and persistently bind to 6Z0P under the current simulation conditions. On the other hand, Luteolin shows a low RMSD, persistent H-bonds, and consistent Rg/SASA values, indicating a stably bound mode and a good inhibitor for the 6Z0P. As for Purpuride, the large RMSD observed in the trajectory, along with the occasional very high per-residue fluctuations, can indicate ligand displacement or ligand conformational change, which renders it a weak inhibitor for 6Z0P. Examination of the trajectory (extracting frames at RMSD peaks) and alignment of the ligand center of mass distance to time plot may provide further evidence of unbinding. Meanwhile, Multidrug efflux transporter BpeB (7WLS): Purpuride shows strong performance: RMSD and Rg are comparable to those of the reference ligand, SASA is moderately attenuated (more buried), and quite clearly the average H-bond count is greater for Purpuride (≈0.94 vs 0.36). RMSF analysis indicates Purpuride decreases local flexibility in several regions compared to the control. Overall, these data suggest that Purpuride is a high-quality binder and a strong potential inhibitor for 7WLS, stabilizing the binding pocket through both hydrogen bonding and favourable packing interactions.

3.5.1.7. Density functional theory study. The electronic structures of Luteolin, 1-(1-naphthylmethyl)piperazine, and Purpuride were optimized at the UB3LYP/6-31 G level of theory. All three ligands successfully converged with RMS gradient norms well below the threshold and no imaginary frequencies, confirming that each optimized geometry corresponds to a true minimum on the potential energy surface. The optimized geometry of Luteolin exhibited a total electronic energy of −1028.3905 a.u. and a dipole moment of 5.99 Debye. Its frontier molecular orbital (FMO) analysis (Fig. 12) revealed HOMO and LUMO energies of −0.3709 a.u. and −0.2208 a.u., respectively, resulting in a HOMO–LUMO gap of 0.1499 a.u. This relatively narrow gap indicates moderate electronic reactivity and a potential for charge-transfer interactions with target proteins.

For 1-(1-naphthylmethyl)piperazine, the optimized structure had an electronic energy of −691.5139 a.u. and the highest dipole moment (7.89 Debye) among the studied ligands, reflecting pronounced polarity and the potential for strong hydrogen-bonding interactions. The HOMO (−0.3321 a.u.) and LUMO (−0.1589 a.u.) values yield an energy gap of 0.1732 a.u., indicating relatively higher stability but lower reactivity compared to Luteolin.

The optimized structure of Purpuride displayed the lowest total energy (−1288.4625 a.u.) and the most stable convergence, as indicated by its minimal RMS gradient norm (0.00000261 a.u.). With a dipole moment of 5.34 Debye, Purpuride exhibited balanced polarity. Its frontier orbital energies (HOMO: −0.4004 a.u., LUMO: −0.2117 a.u.) yielded the largest HOMO–LUMO gap (0.1887 a.u.) among the three ligands, suggesting strong kinetic stability and a lower propensity for electronic excitation.

Overall, while Luteolin and 1-(1-naphthylmethyl)piperazine demonstrated narrower orbital gaps and higher chemical reactivity, Purpuride stood out due to its lowest total energy, favourable electronic configuration, and superior thermodynamic stability. These features support Purpuride as a robust candidate for downstream molecular docking and MD simulation analyses. A comparative summary of the key electronic descriptors for all three ligands is provided in Table 6.

4. Conclusion

This study identified VDRP in *Burkholderia* species and reported that Purpuride compound, identified in the red pigment of *Talaromyces marneffei* strain SA2a, possessed good ADMET and pharmacokinetic properties. Although it had a low half-life and P-glycoprotein properties, Purpuride demonstrated a good binding affinity and formed strong interactions with amino acids at the active site of BVDRP, compared to the reference inhibitors. The molecular dynamics simulation 100 ns showed that Purpuride is a very poor binder for 6Z0P, unlike Luteolin, which showed a low RMSD, persistent H-bonds, and consistent Rg/SASA values. Purpuride shows to be a high-quality binder for 7WLS with strong performance of RMSD, Rg, SASA, H-bond count compared to the reference ligand 1-(1-naphthylmethyl)piperazine. The Luteolin and 1-(1-naphthylmethyl)piperazine demonstrated narrower orbital gaps and higher reactivity. Purpuride stood out due to its lowest total energy, favorable electronic distribution, and superior stability for 7WLS. These characteristics and the binding affinity suggest that Purpuride is a better inhibitor of the *Burkholderia pseudomallei* Multidrug efflux transporter BpeB protein (7WLS), which is responsible for drug efflux in *B. pseudomallei,* compared to the reference ligand -(1-naphthylmethyl) piperazine. Meanwhile, the reference ligand Luteolin is a strong potential inhibitor of *Burkholderia cepacia* BceF Tyrosine Kinase Domain protein (6Z0P), which is responsible for biofilm formation in *B. cepacia*. This Purpuride could be a promising agent for reducing drug resistance in *B. pseudomallei*. This study suggests that further research should be conducted on the potential use of Purpuride in drug development for treating infections caused by *Burkholderia* species.

Funding

The authors did not receive support from any organization for the submitted work.

Declarations

Ethics approval and consent to participate

This article contains no studies with human participants or animal studies.

Consent for publication

All authors have approved the manuscript for publication.

CRediT authorship contribution statement

Alabi Peter Dare: Writing – original draft, Data curation, Conceptualization. **Abideen Akinkunmi Wahab:** Writing – review & editing, Supervision. **Rahul Kumar Singh:** Visualization, Software, Methodology, Formal analysis. **Gbolahan Oladipupo Oduselu:** Visualization, Validation, Software. **Favour Emmanuel Adeloye:** Methodology. **Deborah Temitope Olalekan:** Writing – review & editing, Validation,

Table 6
Quantum chemical parameters of Luteolin, 1-(1-naphthylmethyl)piperazine, and Purpuride obtained from DFT calculations at the UB3LYP/6-31 G level of theory.

Ligand	Total Energy (a.u.)	Dipole Moment (Debye)	HOMO (a.u.)	LUMO (a.u.)	HOMO–LUMO Gap (a.u.)	Point Group
Luteolin	−1028.3905	5.99	−0.3709	−0.2208	0.1499	C1
1-(1-Naphthylmethyl)piperazine	−691.5139	7.89	−0.3321	−0.1589	0.1732	C1
Purpuride	−1288.4625	5.34	−0.4004	−0.2117	0.1887	C1

Data curation. **Folasade Muibat Adeyemi:** Writing – review & editing. **Nana Aishat Yusuf-Omoloye:** Writing – review & editing. **Rukayya Bushola Shittu:** Methodology.

Declaration of competing interest

The authors declare that they have no known competing financial interests or personal relationships that could have appeared to influence the work reported in this paper.

Acknowledgments

The authors acknowledged the support of African Centre of Excellence for Microbial Secondary Metabolites, Osun State University, Osogbo, Nigeria.

Supplementary materials

Supplementary material associated with this article can be found, in the online version, at doi:10.1016/j.insi.2025.100142.

Data availability

The datasets generated for this study are available upon request.

References

[1] Dare AP, Wahab AA, Oyebanji IA, Adeyemi FM, Yusuf-Omoloye NA, Shittu RB. Antimicrobial and antibiofilm forming activities of red pigment of *Talaromyces marneffei* strain SA2a on multidrug-resistant *Burkholderia* sp. UNIOSUN J Eng Environ Sci 2025;7(1):281–306.
[2] Hall CM, Baker AL, Sahl JW, Mayo M, Scholz HC, Kaestli M, Wagner DM. Expanding the *Burkholderia pseudomallei* complex with the addition of two novel species: *burkholderia mayonis* sp. nov. and *Burkholderia savannae* sp. nov. Appl Environ Microbiol 2022;88(1). e01583-21.
[3] Kato T, Okada U, Hung LW, Yamashita E, Kim HB, Kim CY, Murakami S. Crystal structures of multidrug efflux transporters from *Burkholderia pseudomallei* suggest details of transport mechanism. Pro Nat Acad Sci 2022;120(29):e2215072120.
[4] Lauman P, Dennis JJ. Advances in phage therapy: targeting the *Burkholderia cepacia* complex. Viruses 2021;13(7):1331.
[5] Podnecky NL, Rhodes KA, Schweizer HP. Efflux pump-mediated drug resistance in *Burkholderia*. Front Microbiol 2015;6:305.
[6] Chan YY, Tan TM, Ong YM, Chua KL. BpeAB-OprB, a multidrug efflux pump in *Burkholderia pseudomallei*. Antimicrob Agents Chemother 2004;48(4):1128–35.
[7] Kumar A, Chua KL, Schweizer HP. Method for regulated expression of single-copy efflux pump genes in a surrogate *Pseudomonas aeruginosa* strain: identification of the BpeEF-OprC chloramphenicol and trimethoprim efflux pump of *Burkholderia pseudomallei* 1026b. Antimicrob Agents Chemother 2006;50(10):3460–3.
[8] Mima T, Schweizer HP. The BpeAB-OprB efflux pump of *Burkholderia pseudomallei* 1026b does not play a role in quorum sensing, virulence factor production, or extrusion of aminoglycosides but is a broad-spectrum drug efflux system. Antimicrob Agents Chemother 2010;54(8):3113–20.
[9] Somprasong N, Yi J, Hall CM, Webb JR, Sahl JW, Wagner DM, Schweizer HP. Conservation of resistance-nodulation-cell division efflux pump-mediated antibiotic resistance in *Burkholderia cepacia* complex and *Burkholderia pseudomallei* complex species. Antimicrob Agents Chemother 2021;65(9):10–1128.
[10] Selvam K, Khalid MF, Mustaffa KMF, Harun A, Aziah I. BipD of *Burkholderia pseudomallei*: structure, functions, and detection methods. Microorganisms 2021;9(4):711.
[11] Vander Broek CW, Stevens JM. Type III secretion in the melioidosis pathogen *Burkholderia pseudomallei*. Front Cell Inf Microbiol 2017;7:255.
[12] Cozzone AJ. Bacterial tyrosine kinases: novel targets for antibacterial therapy? Trends Microbiol 2009;17(12):536–43.
[13] Grangeasse C, Nessler S, Mijakovic I. Bacterial tyrosine kinases: evolution, biological function and structural insights. Philos Trans R Soc B Biol Sci 2012;367(1602):2640–55.
[14] Mayer M, Matiuhin Y, Nawatha M, Tabachnikov O, Fish I, Schutz N, Landau M. Structural and functional insights into the biofilm-associated BceF tyrosine kinase domain from *Burkholderia cepacia*. Biomolecules 2021;11(8):1196.
[15] Ferreira AS, Leitao JH, Sousa SA, Cosme AM, Sá-Correia I, Moreira LM. Functional analysis of *Burkholderia cepacia* genes *bceD* and *bceF*, encoding a phosphotyrosine phosphatase and a tyrosine autokinase, respectively: role in exopolysaccharide biosynthesis and biofilm formation. Appl Environ Microbiol 2007;73(2):524–34.
[16] Grangeasse C, Cozzone AJ, Deutscher J, Mijakovic I. Tyrosine phosphorylation: an emerging regulatory device of bacterial physiology. Trends Biochem Sci 2007;32(2):86–94.
[17] Papp-Wallace KM, Taracila MA, Gatta JA, Ohuchi N, Bonomo RA, Nukaga M. Insights into β-lactamases from *Burkholderia* species, two phylogenetically related yet distinct resistance determinants. J Biol Chem 2013;288(26):19090–102.
[18] Somprasong N, Hall CM, Webb JR, Sahl JW, Wagner DM, Keim P, Schweizer HP. *Burkholderia ubonensis* meropenem resistance: insights into distinct properties of class A β-lactamases in *Burkholderia cepacia* complex and *Burkholderia pseudomallei* complex bacteria. mBio 2020;11(2):10–1128.
[19] Morgan RE, Batot GO, Dement JM, Rao VA, Eadsforth TC, Hunter WN. Crystal structures of *Burkholderia cenocepacia* dihydropteroate synthase in the apo-form and complexed with the product 7, 8-dihydropteroate. BMC Struct Biol 2011;11:1–9.
[20] Bermingham A, Derrick JP. The folic acid biosynthesis pathway in bacteria: evaluation of potential for antibacterial drug discovery. Bioessays 2002;24(7):637–48.
[21] McCULLOUGH JL, Maren TH. Inhibition of dihydropteroate synthetase from *Escherichia coli* by sulfones and sulfonamides. Antimicrob Agents Chemother 1973;3(6):665–9.
[22] Dennehy R, Romano M, Ruggiero A, Mohamed YF, Dignam SL, C Mujica Troncoso, McClean S. The *Burkholderia cenocepacia* peptidoglycan-associated lipoprotein is involved in epithelial cell attachment and elicitation of inflammation. Cell Microbiol 2017;19(5):e12691.
[23] Godlewska R, Wiśniewska K, Pietras Z, EK Jagusztyn-Krynicka. Peptidoglycan-associated lipoprotein (Pal) of gram-negative bacteria: function, structure, role in pathogenesis and potential application in immunoprophylaxis. FEMS Microbiol Letters 2009;298(1):1–11.
[24] Nikaido H. Molecular basis of bacterial outer membrane permeability revisited. Microbiol Mol Biol Rev 2003;67(4):593–656.
[25] Siritapetawee J, Prinz H, Krittanai C, Suginta W. Expression and refolding of Omp38 from *Burkholderia pseudomallei* and *Burkholderia thailandensis*, and its function as a diffusion porin. Biochem J 2004;384(3):609–17.
[26] Lei LR, Gong LQ, Jin MY, Wang R, Liu R, Gao J, Deng Y. Research advances in the structures and biological activities of secondary metabolites from *talaromyces*. Front Microbiol 2022;13:984801.
[27] George TK, Joy A, Divya K, Jisha MS. *In vitro* and *in silico* docking studies of antibacterial compounds derived from endophytic *penicillium setosum*. Microb Pathog 2019;131:87–97.
[28] Musa A, Abdelgawad MA, Shaker ME, El-Ghorab AH, Parambi DGT, Hamed AA, Aboseada MA. Screening and molecular docking of bioactive metabolites of the Red Sea sponge *callyspongia siphonella* as potential antimicrobial agents. Antibiotics 2022;11(12):682.
[29] Satpathy R. *In-silico* prediction of drug target, molecular modeling, and docking study of potential inhibitors against *Burkholderia pseudomallei*. J Biochem Technol 2023;14:13–21.
[30] Saqallah FG, Hamed WM, Talib WH, Dianita R, Wahab HA. Antimicrobial activity and molecular docking screening of bioactive components of *Antirrhinum majus* (snapdragon) aerial parts. Heliyon 2022;8(8).
[31] Skariyachan S, Praveen PKU, Uttarkar A, Niranjan V. Computational design of prospective molecular targets for *Burkholderia cepacia* complex by molecular docking and dynamic simulation studies. Proteins: Struct F Bio 2023;91(6):724–38.
[32] Vincent AG, Beckham JT. High-performance computational molecular docking for potential inhibitors of an essential enzyme of *Burkholderia pseudomallei*. FASEB J 2022;36.
[33] Schumacher A, Steinke P, Bohnert JA, Akova M, Jonas D, Kern WV. Effect of 1-(1-naphthylmethyl)-piperazine, a novel putative efflux pump inhibitor, on antimicrobial drug susceptibility in clinical isolates of Enterobacteriaceae other than *Escherichia coli*. J Antimicrob Chemother 2006;57(2):344–8.
[34] Coban AY, Guney AK, Tanriverdi Cayci Y, Durupinar B. Effect of 1-(1-Naphtylmethyl)-piperazine, an efflux pump inhibitor, on antimicrobial drug susceptibilities of clinical *Acinetobacter baumannii* isolates. Curr Microbiol 2011;62(2):508–11.
[35] Anes J, Sivasankaran SK, Muthappa DM, Fanning S, Srikumar S. Exposure to sub-inhibitory concentrations of the chemosensitizer 1-(1-naphthylmethyl)-piperazine creates membrane destabilization in multi-drug resistant *Klebsiella pneumoniae*. Front Microbiol 2019;10:92.
[36] Guo Y, Su H, Yu L, Wang Y, Tian C, Zhang D, Guo Y, Liu M. PknB and STP as potential targets of luteolin in combating *Trueperella pyogenes* infections. Sci Rep 2025;15(1):23830.
[37] Johnson S, Roversi P, Espina M, Olive A, Deane JE, Birket S, Lea SM. Self-chaperoning of the type III secretion system needle tip proteins IpaD and BipD. J Biol Chem 2007;282(6):4035–44.
[38] Aunkham A, Schulte A, Winterhalter M, Suginta W. Porin involvement in cephalosporin and carbapenem resistance of *Burkholderia pseudomallei*. PLoS One 2014;9(5):e95918.
[39] Denesyuk AI, Denessiouk K, Johnson MS, Uversky VN. Alpha and omega classification of β-lactamase/transpeptidase-like superfamily proteins based on the comparison of their structural catalytic cores. Molecules 2025;30(9):2019.
[40] Waterhouse A, Bertoni M, Bienert S, Studer G, Tauriello G, Gumienny R, Heer FT, de Beer TA, Rempfer C, Bordoli L, Lepore R. SWISS-MODEL: homology modelling of protein structures and complexes. Nucleic Acids Res 2018;46(W1):W296–303.
[41] Colovos C, Yeates TO. Verification of protein structures: patterns of nonbonded atomic interactions. Protein Sci 1993;2(9):1511–9.
[42] Lüthy R, Bowie JU, Eisenberg D. Assessment of protein models with three-dimensional profiles. Nature 1992;356(6364):83–5.
[43] Kaminski G, Jorgensen WL. Performance of the AMBER94, MMFF94, and OPLS-AA force fields for modeling organic liquids. J Phys Chem 1996;100(46):18010–3.

[44] Liu Y, Yang X, Gan J, Chen S, Xiao ZX, Cao Y. CB-Dock2: improved protein–ligand blind docking by integrating cavity detection, docking and homologous template fitting. Nucleic Acids Res 2022;50(W1):W159–64.
[45] Wahab AA, IA Ibrahim-Fattah, Dare PA, Oyedara OO, Yusuf-Omoloye NA, Adeyemi FM. Tuber pathogenicity of *macrophomina phaseolina* strain 3 a isolated from rotten cassava tuber from farm lands in Osogbo, Osun State, Nigeria, its virulence genes and ADMET properties. Mol Biol Rep 2024;51(1):882.
[46] Lee J, Cheng X, Jo S, MacKerell AD, Klauda JB, Im W. CHARMM-GUI input generator for NAMD, GROMACS, AMBER, OpenMM, and CHARMM/OpenMM simulations using the CHARMM36 additive force field. Biophys J 2016;110(3):641a.
[47] Vanommeslaeghe K, Hatcher E, Acharya C, Kundu S, Zhong S, Shim J, Darian E, Guvench O, Lopes P, Vorobyov I, Mackerell Jr AD. CHARMM general force field: a force field for drug-like molecules compatible with the CHARMM all-atom additive biological force fields. J Comp Chem 2010;31(4):671–90.
[48] Boonstra S, Onck PR, van der Giessen E. CHARMM TIP3P water model suppresses peptide folding by solvating the unfolded state. J Phys Chem B 2016;120(15):3692–8.
[49] Bullerjahn JT, von Bulow S, Heidari M, Hénin J, Hummer G. Unwrapping NPT simulations to calculate diffusion coefficients. J Chem Theory Comp 2023;19(11):3406–17.
[50] Lu L, Hu H, Hou H, Wang B. An improved B3LYP method in the calculation of organic thermochemistry and reactivity. Comp Theoretical Chem 2013;1015:64–71.
[51] Golestanifar F, Garkani-Nejad Z. *In silico* design and ADMET evaluation of new inhibitors for PIM1 kinase using QSAR studies, molecular docking, and molecular dynamic simulation. Heliyon 2024;10(19).
[52] Noser AA, El-Barbary AA, Salem MM, El Salam HAA, Shahien M. Synthesis and molecular docking simulations of novel azepines based on quinazolinone moiety as prospective antimicrobial and antitumor hedgehog signaling inhibitors. Sci Rep 2024;14(1):3530.
[53] Lee LF, Mariappan V, Vellasamy KM, Lee VS, Vadivelu J. Antimicrobial activity of tachyplesin 1 against *Burkholderia pseudomallei*: an *in vitro* and *in silico* approach. PeerJ 2016;4:e2468.
[54] Zosim V, Mullie C, Peltier F, Potron A, Choquet M. 1-(1-naphthylmethyl)-piperazine inhibition assay successfully rules out efflux pump overexpression in *Acinetobacter baumannii*. Mol Biol Rep 2025;52(1):736.
[55] Tuorkey MJ. Molecular targets of luteolin in cancer. Eur J Canc Prev 2016;25(1):65–76.
[56] Bhuiyan AA, Aboul-Soud MA, Uddin MS, Mazumder K, Akash AR, Aljowaie RM, Giesy JP, Agrawal M, Haque S. GC–MS profiling, *in vitro* and *in silico* antibacterial and antioxidant potential of crude secondary metabolites of an endophytic bacterium isolated from *Enhydra fluctuans* lour. Sci Rep 2025;15(1):31876.
[57] Japti VP, Patil MB, Unger BS, Mallapur SP, Shamnewadi A, Patil VS, Patil S, Desai AV. Network pharmacology-based toxicity, molecular docking, and molecular dynamics analysis of phytoconstituents from roots of *Nerium indicum* L. Pharm Res Modern Chin Med 2025;16:100640.
[58] Thapa S, Maurya SN, Manjunath K, Devi K, Varghese SA, Lamsal A, Tamang B, Biradar MS. LC-MS profiling and multi-target mechanistic insights of Hibiscus rosa-sinensis in diabetes: network pharmacology, molecular docking, MD simulation, PCA, and *in-vitro* α-amylase inhibition. Pharm Res Modern Chin Med 2025;16:100636.
[59] Adedeji E.O., Ogunlana O.O., Oduselu G.O., Koenig R., Adebiyi E., Soremekun O.S., Fatumo S. Molecular docking and molecular dynamics simulation studies of inhibitor candidates against *Anopheles gambiae* 3-hydroxykynurenine transaminase and implications on vector control. Heliyon. 2025;11(1).